An Introduction to Propagation, Time Reversal and Imaging in Random Media

Albert C. Fannjiang*
Department of Mathematics, University of California, Davis, CA 95616-8633

Contents

*Electronic address: fannjiang@math.ucdavis.edu

I. SCALAR DIFFRACTION THEORY

A. Introduction

One of the most useful partial differential equations in applied mathematics is the (scalar or vector) wave equation. It describes propagation of linear waves and has a great variety of applications some of which will be discussed below. For instance, the acoustic wave is governed by the scalar wave equation while the electromagnetic wave in dielectric media is governed by the vector wave equation for its vector potential. In media such as the earth's turbulent atmosphere there is negligible depolarization. Thus, by restricting the source to be linearly polarized or by considering two orthogonal polarization components independently, the scalar wave equation is suitable. In this review, we will focus on the scalar waves. Main references for this topic include [3], [43].

Monochromatic waves correspond to the time-harmonic solution $u(\mathbf{r})e^{-i\omega t}$ where ω is the frequency. The spatial component u then satisfies reduced wave equation is

$$\Big[\nabla^2 + k^2(1+\tilde{\epsilon}(\mathbf{r}))\Big]u = f, \quad \mathbf{r} \in \mathbb{R}^3 \tag{1}$$

where f represents source, $\tilde{\epsilon}$ the deviation from the constant background and $k = 2\pi/\lambda$ the wavenumber. Suitable boundary conditions are required to solve eq. (1). $\tilde{\epsilon}$ is related to the relative fluctuation of index of refraction $\tilde{n}$ as $\tilde{\epsilon} \approx 2\tilde{n}$ for $\tilde{n} \ll 1$.

The free, undisturbed propagation is described by the free-space Green function

$$G_0(\mathbf{r}, \mathbf{r}') = -\frac{1}{4\pi|\mathbf{r}-\mathbf{r}'|}e^{ik|\mathbf{r}-\mathbf{r}'|}$$

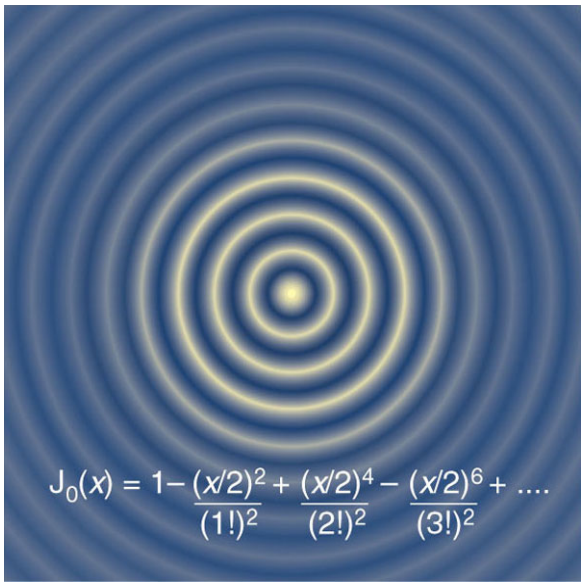

FIG. 1: Non-diffracting Bessel beam with $m = 0$ (adapted from [36]).

which solves

$$\left[\nabla^2 + k^2\right] G_0 = \delta(\mathbf{r})$$

and satisfies the outward radiation condition

$$\left|\frac{\partial G_0}{\partial r} - ikG_0\right| = O(\frac{1}{r^2}), \quad r = |\mathbf{r}|.$$

The wave field u should satisfy the same radiation condition at far field.

Two main phenomena are present when there are multiple sources or fluctuations in the medium: diffraction and interference.

It is important to realize that there is no physical difference between interference and diffraction. However, it is traditional to consider a phenomenon as interference when it involves the superposition of only a few waves, and as diffraction when a large number of waves are involved.

Another aspect that is important to understand is that every optical instrument only uses a portion of the full incident wavefront. Because of this, diffraction plays a significant role in the detailed understanding of the light train through the device. Even in all of the potential defects in the lens system were eliminated, the ultimate sharpness of the image would be limited by diffraction.

In the modern treatment, diffraction effects are not connected with light transmission through apertures and obstacles only. Diffraction is examined as a natural property of wavefield with the nonhomogeneous transverse intensity distribution. It commonly appears even if the beam is transversally unbounded. The Gaussian beam is the best known example.

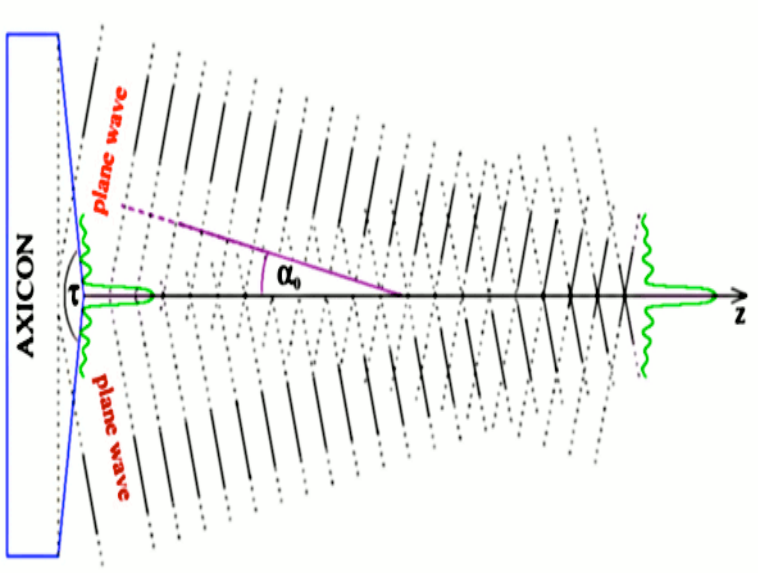

FIG. 2: A Bessel beam is formed after an incident plane wave passes through a conical lens.

In optics, nondiffracting propagation of the beam-like fields can be obtained in convenient media such as waveguides or nonlinear materials. The beams then propagate as waveguide modes and spatial solitons, respectively. In the *free* space, one can easily verify that the field

$$u(\rho, z) = e^{i\beta z} \int_0^{2\pi} A(\phi) e^{i\alpha(x\cos\phi + y\sin\phi)} d\phi, \quad \rho = \sqrt{x^2 + y^2}, \tag{2}$$

with $\alpha^2 + \beta^2 = k^2$ and an arbitrary, complex-valued A satisfies the Helmholtz equation. The choice of $A = 1/(2\pi)$ leads to the zeroth order Bessel beam

$$u(\rho, z) = e^{i\beta z} J_0(\alpha\rho)$$

where J_0 is the zeroth order Bessel function. Such a beam is non-diffracting because the intensity distribution on the transverse plane does not change with the distance of propagation. More generally, we have the higher-order non-diffracting beams

$$u(\rho, \phi, z) = J_m(\alpha\rho) e^{im\phi} e^{i\beta z}, \quad m \in \mathbb{N}$$

[13]. The most useful case is $m = 0$ which gives rise to a cental bright spot.

Formula (2) suggests that a Bessel beam can be formed by a plane wave passing through an axicon, Fig. 2. The summation, or interference of all these waves leads to a bright spot in the centre of the beam. However, since $J_0^2(\alpha\rho)$ decays like $1/\rho$, a Bessel beam requires infinite energy and can not be physically realized exactly. Still, experimental approximations to Bessel beams have extremely low divergence, and are therefore very useful in many applications, specifically in optical tweezers, where an extremely tightly focused hollow beam is optimal.

B. Kirchhoff's theory of diffraction

As said, diffraction corresponds to boundary value problem for the reduced wave equation. For simplicity we consider first the free space with $\tilde{\epsilon} = 0$.

Let a point source be situated at the origin. Green's second identity says that for any $u, v \in C^2$

$$\int_D \left[v\nabla^2 u - u\nabla^2 v\right] d\mathbf{r}_0 = \int_{\partial D} \left[v\frac{\partial u}{\partial n} - u\frac{\partial v}{\partial n}\right] d\sigma(\mathbf{r}_0) \tag{3}$$

where D is the domain of interest, say the space behind an aperture or obstacle. For a fixed probing point $\mathbf{r}$ consider the test function

$$v = \frac{e^{ikr'}}{r'}, \quad r' = |\mathbf{r} - \mathbf{r}_0|$$

on the punctured-at-$\mathbf{r}$ domain D where r' the distance between the point of probing $\mathbf{r}$ and the point of integration $\mathbf{r}_0$. Due to the radiation condition, the far-field boundary on the right hand side of (3) would not contribute at all. And we can use (3) for an unbounded domain D.

Consider the finite boundary $S \cup A$ where S is the (black) screen and A the aperture (pupil). St. Venant's hypothesis states that the optical field in an aperture is the same as if the aperture were not present and $u = 0$ on the screen. Kirchhoff's hypothesis is even stronger

$$\begin{array}{ll} A: & u = u_i, \frac{\partial u}{\partial n} = \frac{\partial u_i}{\partial n} \quad \text{(free, undisturbed propagation)} \\ S: & u = 0, \frac{\partial u}{\partial n} = 0, \quad \text{(vanishing excitation, black screen)} \end{array}$$

where $u_i = 4\pi a G_0$ is the incident wave assuming a point source of strength a. With it, we obtain

$$u(\mathbf{r}) \;=\; -\int_A \left[G_0(\mathbf{r}, \mathbf{r}_0)\frac{\partial u_i}{\partial n} - u_i\frac{\partial G_0(\mathbf{r}, \mathbf{r}_0)}{\partial n}\right] d\sigma(\mathbf{r}_0). \tag{4}$$

Since the problem is linear, eq. (4) holds for an arbitrary incident wave u_i.

Kirchhoff's diffraction formula is an exact solution of the Helmholtz equation but does *not* satisfy Kirchhoff's boundary conditions exactly since one can specify only the Dirichlet or the Neumann condition, but not both in general. In a sense, Kirchhoff's formula is not self-consistent but it is a good approximation when the aperture is sufficiently large and the field point is sufficiently away from the aperture/screen as compared with the wavelength and when the diffraction angle is small. As such, Kirchhoff theory can be viewed as attempt to turn the boundary value problem into an *initial value* problem with data posed on the screen and aperture.

Self-consistency can be obtained so that only one boundary condition is specified but nothing essential is gained. For example one can consider the following test functions for a

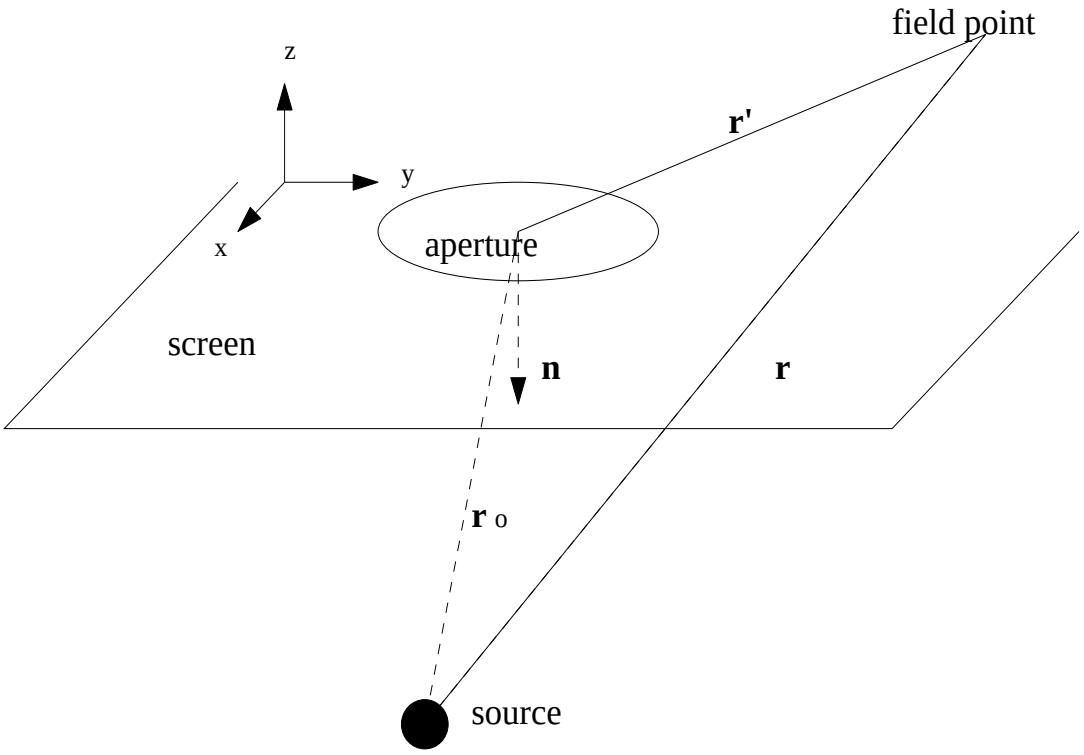

FIG. 3: Geometry of a diffracting aperture

planar diffracting surface

$$v = \frac{e^{ikr_1'}}{r_1'} \mp \frac{e^{ikr_2'}}{r_2'}, \quad r_1' = |\mathbf{r} - \mathbf{r}_0|, \quad r_2' = |\mathbf{r}_i - \mathbf{r}_0|$$

where r_1' is the distance between the field point and the point on the diffracting surface, r_2' the distance between the *image* point of the field point and the diffracting surface, $\mathbf{r}_i$ is the image point of $\mathbf{r}$ w.r.t. the planar screen. For such test functions we have $v = 0$ and $\partial v/\partial n = 0$, respectively, on ∂D and therefore

$$\begin{aligned} u(\mathbf{r}) &= -\frac{1}{4\pi}\int_{\partial D} u\frac{\partial v}{\partial n}d\sigma(\mathbf{r}_0) = \frac{1}{2\pi}\int_{\partial D} u\frac{\partial}{\partial n}\frac{e^{ikr_1'}}{r_1'}d\sigma(\mathbf{r}_0) \\ u(\mathbf{r}) &= \frac{1}{4\pi}\int_{\partial D} v\frac{\partial u}{\partial n}d\sigma(\mathbf{r}_0) = -\frac{1}{2\pi}\int_{\partial D} \frac{e^{ikr_1'}}{r_1'}\frac{\partial u}{\partial n}d\sigma(\mathbf{r}_0), \end{aligned}$$

respectively. They are called Rayleigh's diffraction formulae of the first and the second kind, respectively, and solves the Dirichlet and the Neumann boundary value problem, respectively. The Rayleigh diffraction formulae are mathematically consistent but they are limited to

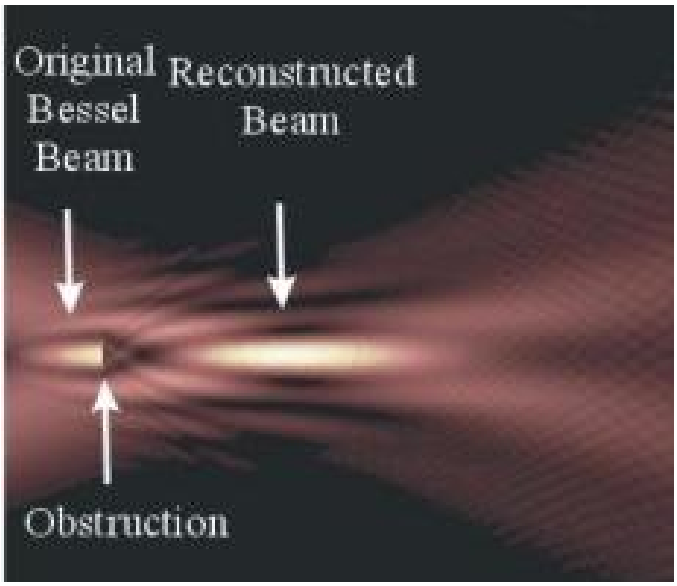

FIG. 4: The beam propagates from left to right. The beam is blocked at the marked position and is seen to reform a short distance later. Credit: David McGloin

planar diffraction surfaces and are not necessarily in closer agreement with observation than the Kirchhoff diffraction formula as the exact boundary values of a black screen is not known [3].

From Green's third identity we know

$$u_i(\mathbf{r}) \;=\; -\int_{\partial D}\left[G_0\frac{\partial u_i}{\partial n} - u_i\frac{\partial G_0}{\partial n}\right]d\sigma$$

and hence

$$u(\mathbf{r}) \;=\; u_i(\mathbf{r}) - \int_S\left[G_0\frac{\partial u_i}{\partial n} - u_i\frac{\partial G_0}{\partial n}\right]d\sigma. \tag{5}$$

This implies Babinet's theorem: Let u_1 be the solution for one setting and u_2 the solution if the aperture and the screens are interchanged. Then, u_1 is the left hand side of (5) and u_2 is the second term on the right hand side of (5). Therefore we have

$$u_1(\mathbf{r}) + u_2(\mathbf{r}) = u_i(\mathbf{r}).$$

Babinet's theorem connects diffraction by an finite obstacle to diffraction through a finite aperture.

Now we apply Babinet's theorem to show the self-repair property of a Bessel beam. Let the incident field u_i be a Bessel beam propagating through an obstacle of a finite extent. The wave field behind the obstacle is u_2 which equals $u_i - u_1$ by Babinet's theorem. The scattered

field u_1, as given by (4) with A being the obstacle, decays like $1/z$ pointwise where z is the distance behind the obstacle. Thus, for a sufficiently large distance u_2 is approximately u_i. In other words, a Bessel beam reforms after passing through an obstacle [5].

Physically, this can be understood as follows. If the bright centre of the beam is distorted it creates a shadow after the distortion. Parts of the light waves far removed from the centre are able to move past the obstacle unhindered and recreate the beam centre at some distance beyond the obstacle. Of course, the same argument applies to an incident, plane wave which is also nondiffracting except the higher intensity at the central spot of a Bessel beam makes this self-repair property more apparent.

C. Huygens-Fresnel principle

Eq. (4) is a manifestation of the Huygens-Fresnel principle of the $3-d$ wave equation, namely every unobstructed point of a wavefront, at a given instant in time, serves as a source of spherical secondary wavelets, with the same frequency as that of the primary wave. The amplitude of the optical field at any point beyond is the superposition of all these wavelets, taking into consideration their amplitudes and relative phases.

First we note that

$$\frac{\partial v}{\partial n} = \tfrac{\partial}{\partial n}\tfrac{e^{ikr'}}{r'} = |\hat{\mathbf{n}}\cdot\hat{\mathbf{r}}'|\frac{\partial}{\partial r'}\frac{e^{ikr'}}{r'} = |\hat{\mathbf{n}}\cdot\hat{\mathbf{r}}'|ik\frac{e^{ikr'}}{r'}\Big(1-\frac{1}{ikr'}\Big), \tag{6}$$

$$\frac{\partial u}{\partial n} = \tfrac{\partial}{\partial n}\tfrac{e^{ikr_0}}{r_0} = -|\hat{\mathbf{n}}\cdot\hat{\mathbf{r}}_0|\frac{\partial}{\partial r_0}\frac{e^{ikr_0}}{r_0} = -|\hat{\mathbf{n}}\cdot\hat{\mathbf{r}}_0|ik\frac{e^{ikr_0}}{r_0}\Big(1-\frac{1}{ikr_0}\Big) \tag{7}$$

It follows that

$$u(\mathbf{r}) = -\frac{a}{4\pi}\int_A \frac{e^{ik(r'+r_0)}}{r_0 r'}ik\Big[|\hat{\mathbf{n}}\cdot\hat{\mathbf{r}}_0|\big(1-\frac{1}{ikr_0}\big)+|\hat{\mathbf{n}}\cdot\hat{\mathbf{r}}'|\big(1-\frac{1}{ikr'}\big)\Big]d\sigma \tag{8}$$

where $r' = |\mathbf{r}-\mathbf{r}_0|$ and $r_0 = |\mathbf{r}_0|$.

We would like to work out a simplification of (8) under the assumption

$$kr_0 \gg 1, \quad kr' \gg 1$$

that is, the Kirchhoff diffraction formula

$$u(\mathbf{r}) = -\frac{ika}{4\pi}\int_A \frac{e^{ik(r'+r_0)}}{r_0 r'}\Big(|\cos\theta_0|+|\cos\theta'|\Big)d\sigma \tag{9}$$

which means that the wave field is the repropagation of the wave front ae^{ikr_0}/r_0 by the Green function G_0 times the inclination factor. We note that this is not the first term of any iterative scheme of the boundary value problem for the reduced wave equation.

For a planar screen we can write $\mathbf{r}' = (z, \mathbf{x} - \mathbf{y})$ where z is the longitudinal coordinate and $\mathbf{x}$ (or $\mathbf{y}$) are the transverse coordinates of the aperture. In the case of *planar* incident wave $u_i = ae^{ikz}$ or a faraway source, then $\theta_0 = 0$ and (9)

$$u(\mathbf{r}) = -\frac{ik}{4\pi} a e^{ikz_0} \int_A \frac{e^{ikr'}}{r'} \Big[1 + \cos\theta'\Big] d\sigma \tag{10}$$

$$= -\frac{ik}{2\pi} a e^{ikz_0} \int_A \frac{e^{ikr'}}{r'} \cos^2 \frac{\theta'}{2} d\sigma. \tag{11}$$

Note that the Kirchhoff diffraction formula does *not* predict $u = 0$ on the screen (i.e. $\theta' = \pi/2$) as does the Rayleigh diffraction formula of the first kind. Instead, the Kirchhoff diffraction formula predicts $u = 0$ in the back-propagation direction (i.e. $\theta' = \pi$).

Using the Huygens-Fresnel principle we can generalize Kirchhoff's formula to the case with arbitrary source and aperture (transmission) function $\tau(\mathbf{r}_0)$

$$u(\mathbf{r}) = -ik \int_A \tau(\mathbf{r}_0) u_i(\mathbf{r}_0) \frac{e^{ikr'}}{r'} \Big(|\cos\theta_0| + |\cos\theta'| \Big) d\sigma(\mathbf{r}_0) \tag{12}$$

where the contribution from θ_0 represents a "history" term.

For example for a thin parabolic lens the aperture (transmission) function is given by

$$\tau(\mathbf{x}) \approx |\tau(\mathbf{x})| e^{-ik|\mathbf{x}|^2/(2f)}.$$

In the case of plano-convex lens we have $f = R/(n-1)$; in the case of bi-convex lens with radii of curvature R_1, R_2 we have

$$\frac{1}{f} = (n-1)\Big(\frac{1}{R_1} + \frac{1}{R_2}\Big).$$

The axicon (Fig. 2) can be replaced with an annular slit (the aperture) at the focal plane of a thin parabolic lens as depicted in Fig. 5. After the incident plane wave passing through the annular slit each point of the slit becomes a point source of a spherical wave which is converted back into a plane wave again with a transverse wavevector given by minus the transverse coordinates of the point on the aperture plane. An annular slit produces the entire set of the wavevectors of an axicon. An incident plane wave corresponds to a constant A in (2) and thus the zeroth order Bessel beam.

D. Fresnel and Frauhoffer diffraction

We derive the Fresnel diffraction formula which is the paraxial approximation of (11) under the small-diffraction-angle condition $A \ll z$. In the Fresnel diffraction one approximates the radius function by the quadratic approximation

$$|\mathbf{r}| \approx z + \frac{|\mathbf{x} - \mathbf{y}|^2}{2z}$$

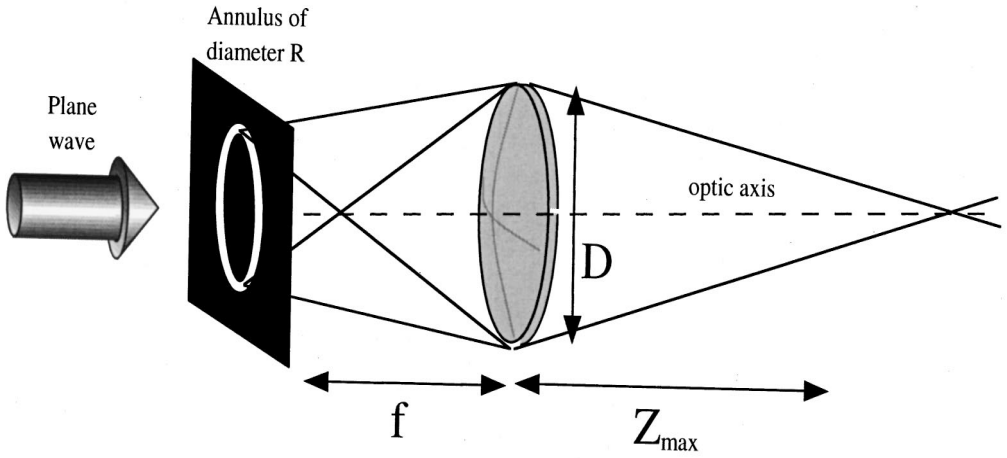

FIG. 5: A He-Ne laser is used to illuminate the annular slit to produce the Bessel beam (adapted from [44])

and set $\theta' = 0$ (hence called "paraxial approximation"). Let $\mathbb{I}_A$ be the indicator function of the aperture and

$$G(z, \mathbf{x}) = e^{ikz} \frac{k}{i2\pi z} \exp\left[i \frac{k}{2z} |\mathbf{x}|^2 \right].$$

Then (11) can be written as

$$u(z, \mathbf{x}) = u_0(\cdot) * G(z, \cdot) \tag{13}$$

where $u_0 = u_i \tau \mathbb{I}_A$. Note that the Fresnel formula (13) satisfies the equation

$$\Big(\frac{\partial}{\partial z} - ik \Big) u = \frac{i}{2k} \Delta_x u \tag{14}$$

with u_0 as initial data.

For far field, the Fraunhofer diffraction formula is a good approximation under the condition $L_f = \sqrt{\lambda z} \gg A$. This means Fresnel number

$$\gamma = \frac{z}{kA^2} \gg 1.$$

This leads to negligible quadratic phase factor and the curvature of the wave front and the approximation of spherical waves by planar waves of different angles (or spatial frequencies):

$$u(z, \mathbf{x}) = e^{ikz} e^{i \frac{k|\mathbf{x}|^2}{2z}} \frac{k}{i2\pi z} \int_A u_0(\mathbf{y}) \exp\left(-i\mathbf{p} \cdot \mathbf{y}\right) d\mathbf{y} \tag{15}$$

with the Fourier variables, called *spatial frequencies*

$$\mathbf{p} = 2\pi \frac{\mathbf{x}}{\lambda z} = \frac{k\mathbf{x}}{z}.$$

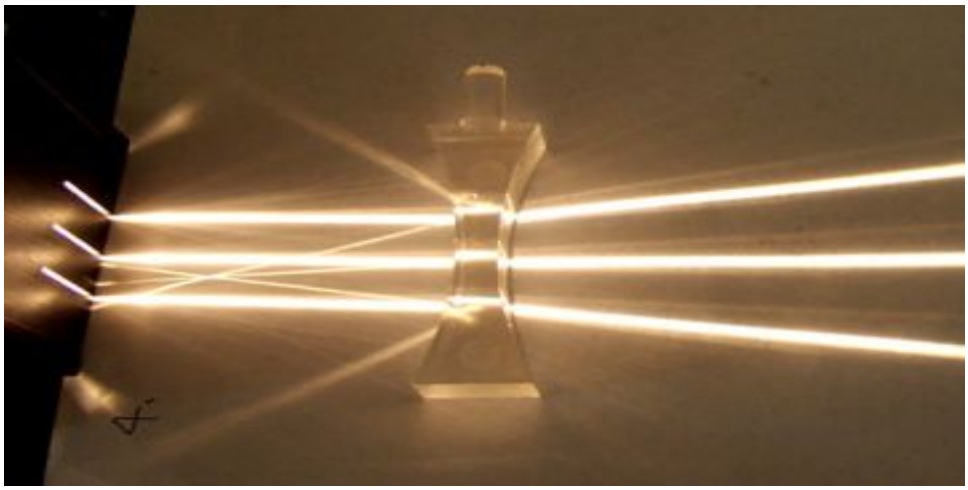

FIG. 6: Concave lens diverges light rays

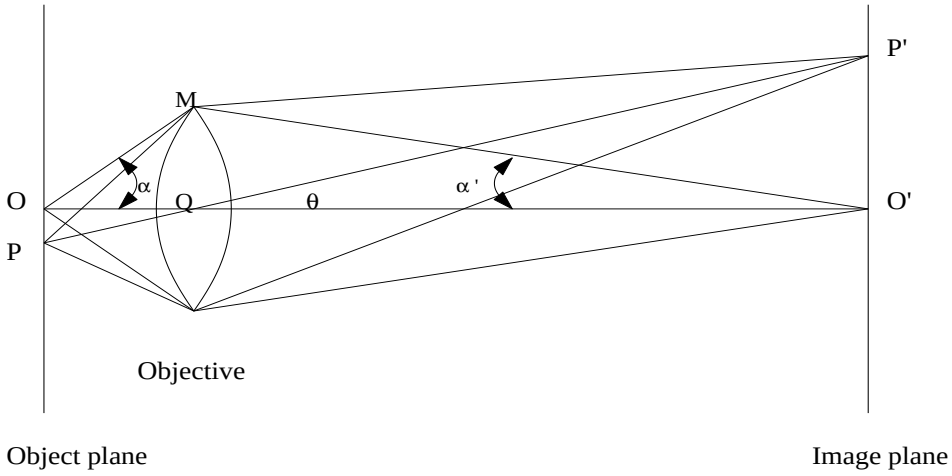

FIG. 7: Ray geometry of a microscope

E. Focal spot size and resolution

Let us consider the Fraunhoffer diffraction by a slit and a circular aperture.

Consider the planar incident wave $u_0 = ae^{ikz}$. Let A be the x-width of the y-infinitely long slit. Then the Fraunhoffer formula amounts to the Fourier transformation of a finite interval of length A modulo a phase factor independent of the transverse variable $\mathbf{x}$. We

obtain

$$|u|^2(x) = |a|^2 \Big| \frac{\sin(pA/2)}{p/2} \Big|^2, \quad p = kx/z$$

which has the minima for $pA/2 = \pm\pi, \pm 2\pi, \cdots$.

The size of the main lobe determines the resolution of the system. We set $pA/2 = \pi$ and obtain

$$\rho = \frac{\lambda z}{A}$$

which is called the Rayleigh (or Abbe) resolution formula. Note that as the derivation relies on (15) the Rayleigh formula is not valid for $z/A \to 0$.

In the case of a circular aperture of diameter A, the Fraunhoffer diffraction formula amounts to the Fourier transform of a circular disk of diameter A modulo a phase factor, i.e.

$$|u|^2(\rho) = |a|^2 \Big| \frac{J_1(kA \tan\theta/2)}{kA \tan\theta/2} \Big|^2$$

where θ is the diffraction angle and

$$J_1(\xi) = \frac{1}{\pi} \int_{-\pi/2}^{\pi/2} \sin(\xi \cos\phi) \cos\phi d\phi$$

is the Bessel function of order one. The first zero of $J_1(\xi)$ is at $\xi = 1.22\pi$. Consequently, the first dark ring occurs at the diffraction angle

$$\tan\theta_1 = 1.22 \frac{\lambda}{A}. \tag{16}$$

For the resolving power of a microscope we need to consider the optical geometry of the instrument as shown in Figure 7. We use the unprimed notion for the quantities on the object plane and the primed notion for those on the image plane. Let us observe the relation

$$\overline{PO} \tan\alpha = \overline{P'O'} \tan\alpha'$$

which follows from the following string of identities

$$\frac{\overline{P'O'}}{\overline{PO}} = \frac{\overline{O'Q}}{\overline{OQ}} = \frac{\overline{O'Q}/\overline{QM}}{\overline{OQ}/\overline{QM}} = \frac{\tan\alpha}{\tan\alpha'},$$

cf. Fig 7. A more accurate relation, called the sine condition,

$$\overline{OP} \sin\alpha = \overline{O'P'} \sin\alpha'. \tag{17}$$

can be derived by using the Fermat principle in geometrical optics [3].

According to Rayleigh's criterion (16) θ needs to be large than θ_1 for P' and O' to be distinguishable. This implies by the sine condition that

$$\overline{OP} > 1.22 \frac{\lambda}{n \tan\alpha}.$$

Therefore the ultimate resolution of a microscope with a circular lens is limited by $1.22\lambda/(2n)$.

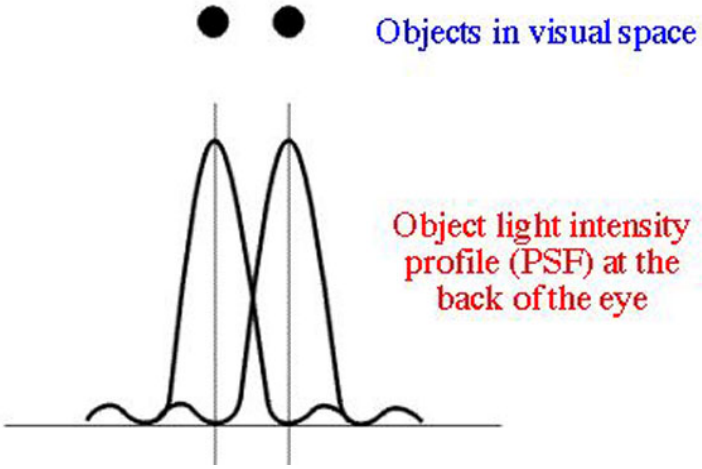

FIG. 8: Rayleigh resolution criterion

II. APPROXIMATIONS: WEAK FLUCTUATION

First we consider several widely used approximation for propagation in the weak fluctuation regime where $\tilde{\epsilon}$ is small.

A. Born approximation

We rewriting (1) in the form

$$(\nabla^2 + k^2)u = -k^2\tilde{\epsilon}u$$

and convert it into the Lippmann-Schwinger integral equation

$$u(\mathbf{r}) = u_0(\mathbf{r}) - k^2 \int G_0(\mathbf{r} - \mathbf{r}')\tilde{\epsilon}(\mathbf{r}')u(\mathbf{r}')d\mathbf{r}'$$

where u_0 is the wave field in the absence of the heterogeneity. This formulation suggests the iteration scheme for solving for u which produces the Born series for u. Substituting u_0 in the right hand side of the above integral we obtain the first term u_1 in the Born series. Repeating this process we can develop the entire Born series.

B. Rytov approximation

The Rytov approximation employs the exponential transformation

$$u(\mathbf{r}) = u_0 e^{\phi}, \tag{18}$$

where u_0 is the solution of the Helmholtz equation in the absence of medium fluctuation, and develop a series solution for ϕ in a way analogous to the Born approximation. The equation for ϕ is

$$(\nabla^2 + k^2)(u_0\phi) + u_0\Big|\nabla\phi\Big|^2 + k^2\tilde{\epsilon}u_0 = 0.$$

Note that the equation is nonlinear but the multiplicative heterogeneity becomes additive.

Once again we can formulate the equation as the integral equation

$$\phi(\mathbf{r}) = -\frac{1}{u_0(\mathbf{r})}\int G_0(\mathbf{r}-\mathbf{r}')u_0(\mathbf{r}')\Big[\Big|\phi(\mathbf{r}')\Big|^2 + k^2\tilde{\epsilon}(\mathbf{r}')\Big]d\mathbf{r}'$$

and develop a series expansion for ϕ. The Rytov approximation amounts to neglecting the quadratic term in ϕ:

$$\phi_1(\mathbf{r}) = -\frac{k^2}{u_0(\mathbf{r})}\int G_0(\mathbf{r}-\mathbf{r}')u_0(\mathbf{r}')\tilde{\epsilon}(\mathbf{r}')d\mathbf{r}'.$$

The Rytov approximation is consistent with the Born approximation in that the latter is the two-term approximation of $u_0e^{\phi_1} = u_0(1+\phi_1+\cdots)$ in view of the fact $u_0\phi_1 = u_1$. However, the Rytov approximation is generally believed to be superior to the Born approximation for propagation in turbulent media. The Rytov approximation is the basic propagation model in diffractive tomography of which the computerized tomography is a limit case as $k \to \infty$ [47]. One can find a comprehensive treatment of the Rytov method in [56].

More generally, let us divide a heterogeneous medium as a series of thin layers for each of which the Rytov approximation applies. Let u_0 be the incident wave. Then after the 1-st layer the wave field is u_0u_1 where $u_1 = e^{\phi_1}$ is the Rytov solution. For the second layer, u_0u_1 is the incident wave and $u_0u_1u_2$ is the transmitted wave where $u_2 = e^{\phi_2}$. In this way, the total output field becomes $u_0u_1u_2u_3\cdots = u_0\exp(\phi_1+\phi_2+\phi_3+\cdots)$. Namely the exponential representation (18) turns the product of many contributions into a summation which is more convenient to analyze. That is why the Rytov method is more suitable for the so-called line-of-sight propagation. On the other hand, for the single scattering problem where the output field is a sum of contributions from different parts of the medium fluctuation, the sum form $u = u_0 + u_1$ is more suitable [8], [37]. In reality, however, the true picture is the combination of the two.

C. The extended Huygens-Fresnel principle

The extended Huygens-Fresnel principle is the extension of (12) as

$$u(\mathbf{r}) = -2ik\int u_i(\mathbf{r}_0)G_0(\mathbf{r}-\mathbf{r}_0)e^{\phi_1(\mathbf{r},\mathbf{r}_0)}\cos^2\frac{\theta'}{2}d\sigma \tag{19}$$

where ϕ_1 is the first Rytov approximation.

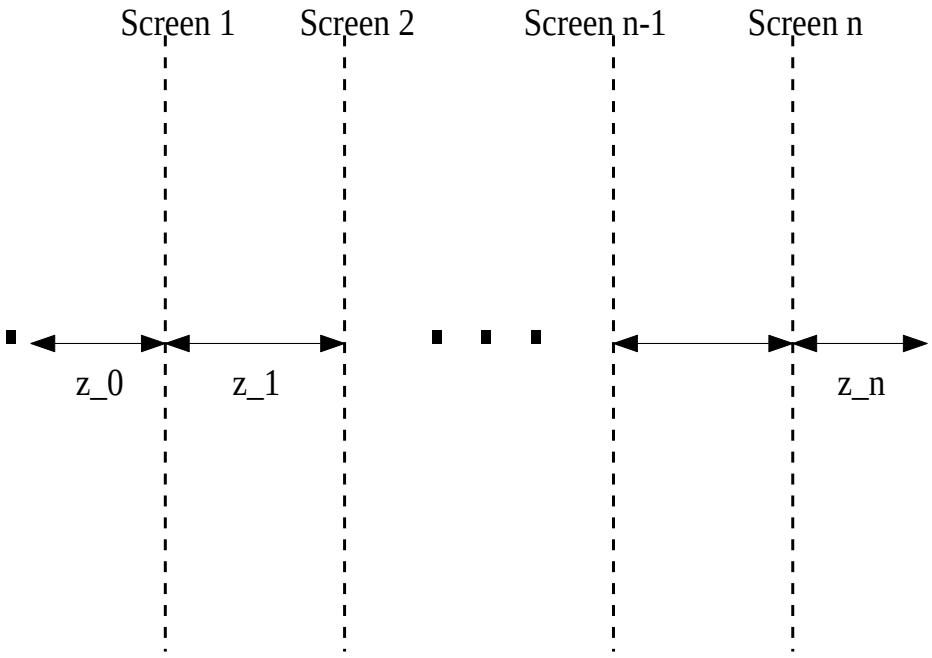

FIG. 9: Multiple phase screens

In the paraxial regime (19) can be approximated by

$$u(\mathbf{r}) \;=\; -\frac{ik}{2\pi z}\int e^{ikz}e^{i\frac{k|\mathbf{x}-\mathbf{x}_0|^2}{2z}}e^{\phi_1}u_i(\mathbf{r}_0)d\sigma. \tag{20}$$

A useful application of the Huygens-Fresnel principle is in treating the case where the extended medium can be approximated by a series of phase screens. A phase screen is defined as having the transmission function of the form $\tau(\mathbf{x}) = e^{\phi(\mathbf{x})}$ where ϕ may be complex-valued and zero reflection coefficient. Mathematically this amounts to the forward-scattering (or paraxial) approximation [38], [14].

Consider a series of phase screens with the transmission functions $\tau_j = e^{i\phi_j}$ as in Fig. 9. By iterating the extended Huygens-Fresnel principle we obtain the wave field at the end of the screens [54]

$$u(z,\mathbf{x}) = \int d\mathbf{x}_0 \cdots \int d\mathbf{x}_n u_i(\mathbf{x}_0)e^{\phi_1+\cdots+\phi_n}G_0(z_0,\mathbf{x}_1-\mathbf{x}_0)G_0(z_1,\mathbf{x}_2-\mathbf{x}_1)\cdots G_0(z_n,\mathbf{x}-\mathbf{x}_n).$$

The concept of phase screen is not restricted to electromagnetic wave propagation. For example, the basis of image formation in the transmission electron microscope is the interaction of the electron with the object. In most applications, the elastic scattering interaction can be described as phase shift of the incident wave traveling in the z direction

$$\Phi(\mathbf{x}) = \int C(z,\mathbf{x})dz \tag{21}$$

where $C(z, \mathbf{x})$ is the Coulomb potential within the object and the incident wave u_0 is modified according to

$$u(\mathbf{x}) = u_0 e^{i\Phi(\mathbf{x})}.$$

In contrast, tomography concerns mostly the inelastic scattering (absorption). The Born approximation would then lead to $u = u_0(1 + i\Phi)$ [32]. In diffraction theory, a *field*, rather than a material object, can often be modeled as a *phase* object, cf. Section VII A.

D. Paraxial approximation

The forward-scattering (or paraxial) approximation concerns the propagation of modulated high-frequency carrier wave written as

$$E(\mathbf{x}) = \Psi(z, \mathbf{x}) e^{ikz}$$

with $k \gg 1$. The equation for Ψ is

$$\frac{\partial^2}{\partial z^2}\Psi + \nabla_\perp^2 \Psi + 2ik\frac{\partial}{\partial z}\Psi + 2k^2\tilde{n}\Psi = 0 \tag{22}$$

where $\tilde{n}$ is the relative fluctuation of the index of refraction. Then under the assumption

$$|\Psi_{zz}| \ll 2k|\Psi_z|,$$

we obtain

$$i\frac{\partial}{\partial z}\Psi + \frac{1}{2k}\Delta\Psi + k\tilde{n}\Psi = 0 \tag{23}$$

which is analogous to the Fresnel approximation (14).

A more formal approach is to factorize eq. (22) as

$$\Big(\frac{\partial}{\partial z} + ik + ikQ\Big)\Big(\frac{\partial}{\partial z} + ik - ikQ\Big)\Psi + ik\Big[Q, \frac{\partial}{\partial z}\Big]\Psi = 0 \tag{24}$$

where

$$Q = \Big(1 + \frac{1}{k^2}\nabla_\perp^2 + 2\tilde{n}\Big)^{1/2}$$

and $\Big[Q, \frac{\partial}{\partial z}\Big] = Q\frac{\partial}{\partial z} - \frac{\partial}{\partial z}Q$ is the commutator. For Q to be well-defined, it is necessary that it acts on a wave field whose maximum transverse wavenumber is smaller than k (i.e. the evanescent waves are negligible) and $\tilde{n}$ is sufficiently small. For weak fluctuation $\tilde{n} \ll 1$ or z-independent $\tilde{n}$ the commutator can be dropped and the remaining equation is the product of two nearly commutative operators describing forward and backward propagating waves.

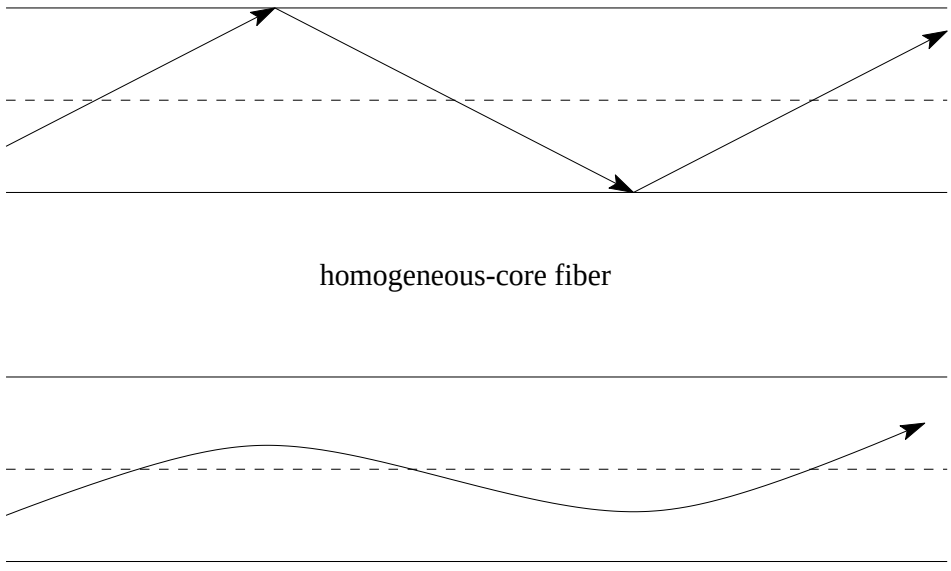

FIG. 10: Homogeneneous vs. graded index wave guide

If only the forward-propagating term of eq. (24) is retained, we have the generalized paraxial wave equation

$$\Big(\frac{\partial}{\partial z} + ik - ikQ\Big)\Psi = 0. \tag{25}$$

The paraxial approximation turns the two-sided boundary value problem for the reduced wave equation into the one-sided initial value problem for the Schrödinger equation [54], [53].

The standard paraxial wave equation is the simplest approximation of (25) by Taylor expanding Q around the identity and using

$$Q' = 1 + \frac{1}{2k^2}\nabla_\perp^2 + \tilde{n}$$

to approximate Q. The resulting equation is (23). Formally this approximation requires that $\tilde{n}$ is small and that the transverse wavenumber of Ψ is much smaller than k (i.e. small diffraction angle).

In the graded-index optical fibers the index of refraction has the profile

$$n^2 = \begin{cases} n_0^2[1 - 2\sigma|\mathbf{x}|^2/a^2], & 0 < |\mathbf{x}| < a \\ n_0^2[1 - 2\sigma], & |\mathbf{x}| > a. \end{cases}$$

Note that in this case $\left[Q, \frac{\partial}{\partial z}\right] = 0$. The parabolic index fiber can reduce pulse dispersion in optical communication because the rays making larger angles with the axis also traverse a larger path length in a region of lower refractive index [33]. In the wave-guide with infinitely extended parabolic profile

$$n^2 = n_0^2\Big[1 - \frac{|\mathbf{x}|^2}{a^2}\Big]$$

the eigenfunctions of the paraxial wave equation can be solved for exactly. The resulting eigenfunctions form a complete and orthogonal set of solutions for the square-integrable functions on the transverse plane. When the transverse coordinate is one-dimensional, the normalized eigenfunctions are the Hermite functions

$$\Psi_m(x) = \sqrt{\frac{1}{\sqrt{\pi}2^m m!}} H_m(x) e^{-\frac{x^2}{2}}, \quad m = 0, 1, 2, ... \tag{26}$$

where $H_j(x)$ stands for the Hermite polynomial of order j

$$H_j(x) = (-1)^j e^{x^2} \frac{d^j}{dx^j} e^{-x^2}$$

or equivalently defined recursively as $H_0(x) = 1, H_1(x) = 2x, H_{j+1}(x) = 2xH_j(x) - 2jH_{j-1}(x)$. A laser beam profile can be decomposed into the so called Hermite-Gaussian modes, each mode being characterized by two integer numbers n and m

$$\mathrm{TEM}_{mn}(x, y) = w(z)^{-1} \Psi_m(\frac{x}{w(z)}) \Psi_n(\frac{y}{w(z)}) e^{-\frac{ik(x^2+y^2)}{2R(z)} - i(kz - \phi_m(z) - \phi_n(z))} \tag{27}$$

where Φ_{mn} is the Guoy phase defined as

$$\phi_m(z) = (m + 1/2) \arctan\left(\frac{\lambda z}{\pi w_0^2}\right).$$

TEM is the acronym for *Transverse Electro-Magnetic* mode, where m refers to the number of intensity minima in the direction of the electric field oscillation, and n refers to the number of minima in the direction of the magnetic field oscillation.

The set of modes is characterized at every point along the propagation axis by two functions: $R(z)$ and $w(z)$ as shown on Fig. 12. The first describes the radius of curvature of the wavefront that intersects the propagation axis, while the second parameter, with respect to the fundamental mode TEM_{00}, gives the radius in the transverse plane for which the amplitude of the field has decreased by a factor e^{-1} with respect to the amplitude value along the propagation axis. The transversal intensity distribution of the TEM_{00} has a Gaussian dependence and its radius $w(z)$ contracts to a minimum w_0 known as the waist of the beam. The two parameters $R(z)$ and $w(z)$ are determined by the waist size w_0 and by the distance

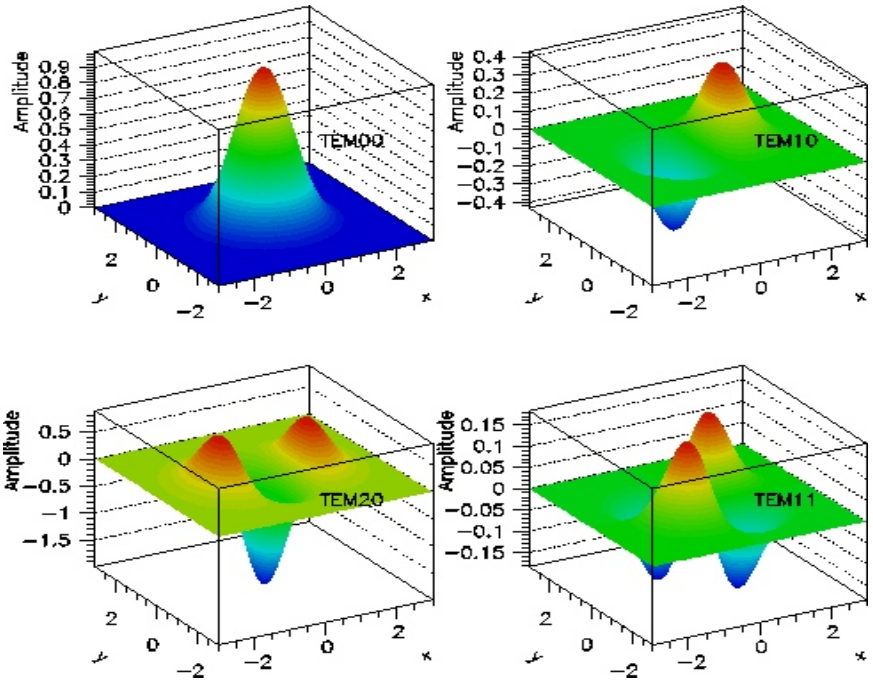

FIG. 11: Graphs of $\mathrm{TEM}_{mn}, m, n = 0, 1$.The fundamental mode TEM_{00} has a Gaussian profile in the transverse plane while TEM_{10} exhibits a left-right asymmetry.

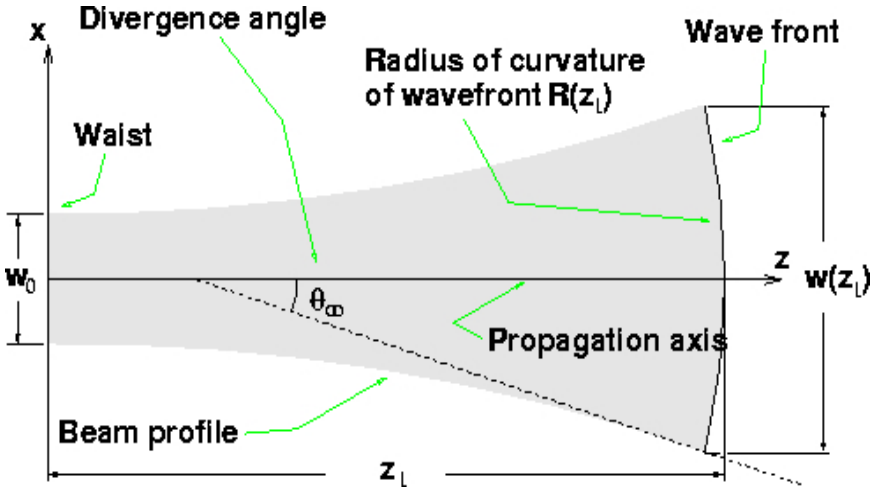

FIG. 12: Longitudinal profile of a laser beam

z from the waist position:

$$w^2(z) \;=\; w_0^2\left[1+\left(\frac{\lambda z}{\pi w_0^2}\right)^2\right] \tag{28}$$

$$R(z) \;=\; z\left[1+\left(\frac{\pi w_0^2}{\lambda z}\right)^2\right]. \tag{29}$$

The longitudinal profile of a laser beam is a hyperbola with asymptotes forming an angle

$$\theta_\infty = \frac{\lambda}{\pi w_0}$$

with the propagation axis, which defines the divergence of the beam.

Nevertheless, the paraxial wave equation is not exactly solvable in general. A general way of understanding and numerical solution of the standard paraxial equation is through the *step-splitting* method. By Trotter's product formula we can write the solution to (23) for a small step as

$$\Psi(z+dz,\mathbf{x}) \approx e^{i\frac{k}{2}\Delta dz}e^{ik\int_z^{z+dz}\tilde{n}(z',\mathbf{x})dz'}\Psi(z,\mathbf{x})$$

The evolution with only $\tilde{n}$ present is the effect of medium fluctuation represented as a simple phase screen in the geometrical optics while the evolution with only Δ present is the diffraction effect in the free space. Thus the entire propagation consists of a series of phase screens separated by uniform medium in between cf. Fig. 9. When dz is greater than the correlation length of medium fluctuation the phase screens can be considered statistically independent. The phase screens cause the fluctuation in phase and the diffraction causes the fluctuation in amplitude (and phase). This algorithm is the discrete analog of path-integral method of the paraxial wave equation in the limit of $dz \to 0$ [54]. Moreover, the multiple phase screen model is not restricted to the paraxial wave equation and can be extended to deal with point source and spherical wave by writing the equation in spherical coordinates.

We will be mostly interested in a randomly heterogeneous medium such as the turbulent atmosphere for which $\tilde{n}(\mathbf{r})$ is a random function. We shall use $\langle\cdot\rangle$ and $\mathbb{E}$ to denote the averaging w.r.t. the ensemble of noise and media, respectively. There are two regimes of interest: the weak fluctuation regime and the strong fluctuation regime and they require different treatments. The weak fluctuation regime can be defined as

$$\frac{\mathbb{E}(I-\mathbb{E}I)^2}{|\mathbb{E}I|^2} < 1, \quad I = |\Psi|^2$$

whose left hand side is also known as the scintillation index. The strong fluctuation regime is when the scintillation index is much larger than one.

III. THE WIGNER DISTRIBUTION

In this section, we discuss a useful phase-space tool for analyzing imaging properties of optical elements [12, 31]. This is a quadratic transform of the wave field.

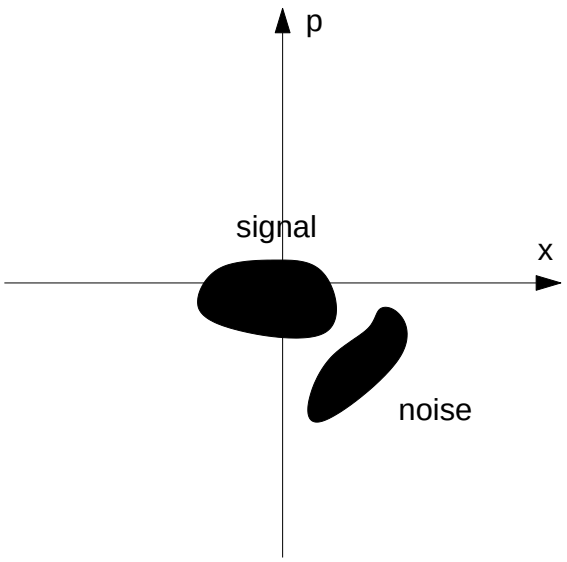

FIG. 13: Signal and noise are more clearly separated in the phase space

The standard Wigner distribution (or transform) for a wave field Ψ is defined as

$$W[\Psi](\mathbf{x},\mathbf{p}) = \frac{1}{(2\pi)^d}\int e^{-i\mathbf{p}\cdot\mathbf{y}}\Psi\left(\mathbf{x}+\frac{\mathbf{y}}{2}\right)\Psi^*\left(\mathbf{x}-\frac{\mathbf{y}}{2}\right)d\mathbf{y} \tag{30}$$

from which the wave amplitude Ψ can be recovered up to a constant phase factor by using

$$\Psi(\mathbf{x}_1)\Psi^*(\mathbf{x}_2) \;=\; \int W[\Psi](\frac{1}{2}(\mathbf{x}_1+\mathbf{x}_2),\mathbf{q})\exp\left[i\mathbf{q}\cdot(\mathbf{x}_1-\mathbf{x}_2)\right]d\mathbf{q}.$$

For example, the Gaussian beam

$$\Psi(x) = Ce^{-\frac{(x-x_0)^2}{2w_0^2}+ip_0x}$$

gives rise to a Gaussian Wigner distribution as shown in Fig. 14.

A motivation for any phase space approach to signal analysis is that the signal and the noise components may otherwise not be clearly separated from each other when projected either on the x or p axis, Fig. 13.

The Wigner distribution is the Fourier transform in the phase space of the ambiguity function

$$A(\mathbf{y},\mathbf{q}) = \frac{1}{(2\pi)^d}\int e^{-i\mathbf{q}\cdot\mathbf{x}}\Psi\left(\mathbf{x}+\frac{\mathbf{y}}{2}\right)\Psi^*\left(\mathbf{x}-\frac{\mathbf{y}}{2}\right)d\mathbf{x}$$

widely used in radar signal processing, also called the Fourier-Wigner transform of Ψ [35]. While the ambiguity function is an expression for correlative structure, the Wigner distribution describes the energy distribution in the phase space. This is manifest in the following

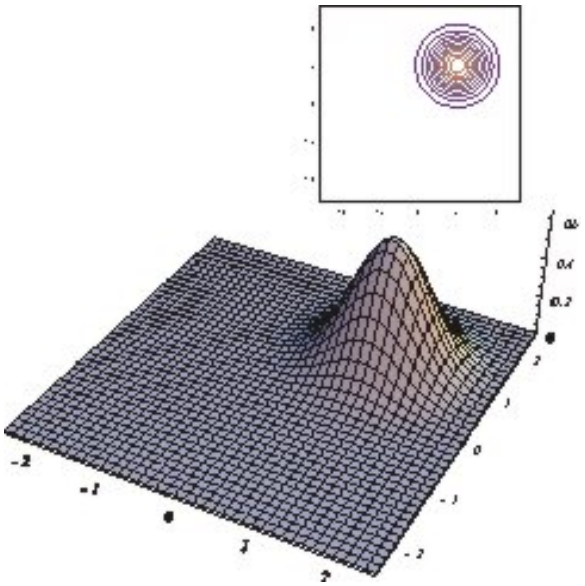

FIG. 14: The Wigner distribution associated with the Gaussian beam.

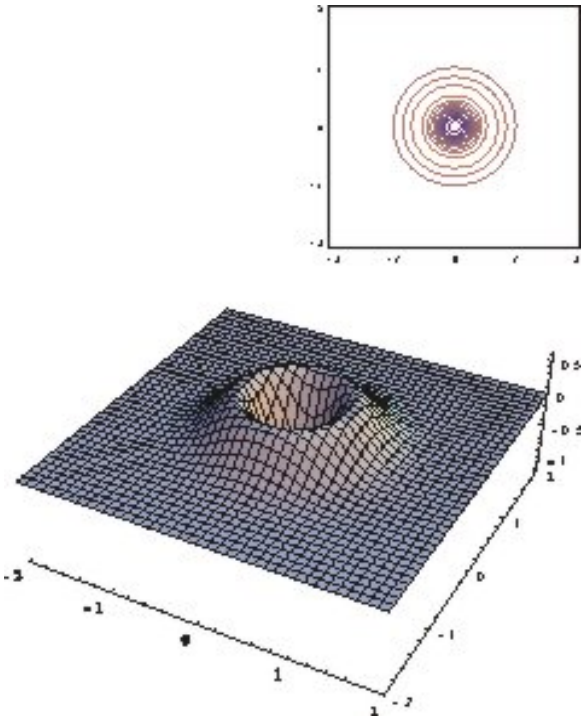

FIG. 15: The Wigner distribution associated with Ψ_1.

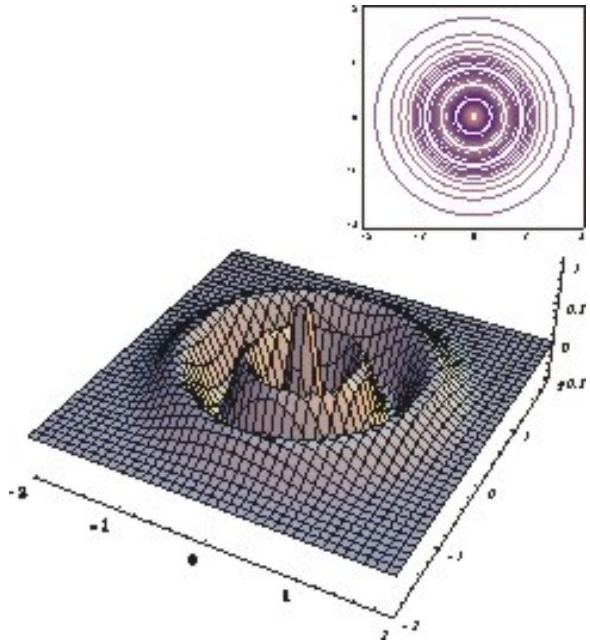

FIG. 16: The Wigner distribution associated with Ψ_4.

properties. For instance, partial integration of W gives rise to the marginal distributions

$$\begin{aligned}\int W[\Psi](\mathbf{x},\mathbf{p})d\mathbf{p} &= |\Psi(\mathbf{x})|^2\\ \int W[\Psi](\mathbf{x},\mathbf{p})d\mathbf{x} &= (2\pi)^d\,|\hat{\Psi}(\mathbf{p})|^2.\end{aligned}$$

Also, the energy flux is given by

$$\frac{1}{2i}(\Psi\nabla\Psi^* - \Psi^*\nabla\Psi) = \int_{\mathbb{R}^d} \mathbf{p}W(z,\mathbf{x},\mathbf{p})d\mathbf{p}. \tag{31}$$

We consider the following operators and their action on the corresponding Wigner distribution.

- Fourier transform $\mathfrak{F}\Psi(\mathbf{k}) = \int e^{-i\mathbf{k}\cdot\mathbf{x}}\Psi(\mathbf{x})d\mathbf{x}$ (Fraunhoffer diffraction).
- Dilation $D_a, a > 0$: $D_a\Psi(\mathbf{x}) = a^{-1}\Psi(\frac{\mathbf{x}}{a})$.
- Symmetry: $S\Psi(\mathbf{x}) = \Psi(-\mathbf{x})$.
- Translation $T_\mathbf{y}, \mathbf{y} \in \mathbb{R}^2$: $T_\mathbf{y}\Psi(\mathbf{x}) = \Psi(\mathbf{x}-\mathbf{y})$.
- Modulation $M_\mathbf{k}, \mathbf{k} \in \mathbb{R}^2$: $M_\mathbf{k}\Psi(\mathbf{x}) = e^{i\mathbf{k}\cdot\mathbf{x}}\Psi(\mathbf{x})$.

- Chirp multiplication $P_{\mathbf{k}}, \mathbf{k} \in \mathbb{R}^2$: $P_{\mathbf{k}}\Psi(\mathbf{x}) = e^{i|\mathbf{k}||\mathbf{x}|^2}\Psi(\mathbf{x})$ (Lens effect)
- Chirp convolution $Q_{\mathbf{k}}, \mathbf{k} \in \mathbb{R}^2$: $Q_{\mathbf{k}}\Psi(\mathbf{x}) = e^{i|\mathbf{k}||\mathbf{x}|^2} \star \Psi(\mathbf{x})$ (free space propagation).

We have

- $W[\mathfrak{F}\Psi](\mathbf{x}, \mathbf{p}) = W[\Psi](-\mathbf{p}, \mathbf{x})$
- $W[D_a\Psi](\mathbf{x}, \mathbf{p}) = W[\Psi](\frac{\mathbf{x}}{a}, a\mathbf{p})$
- $W[S\Psi](\mathbf{x}, \mathbf{p}) = W[\Psi](-\mathbf{x}, -\mathbf{p})$
- $W[T_{\mathbf{y}}\Psi](\mathbf{x}, \mathbf{p}) = W[\Psi](\mathbf{x} - \mathbf{y}, \mathbf{p})$
- $W[M_{\mathbf{q}}\Psi](\mathbf{x}, \mathbf{p}) = W[\Psi](\mathbf{x}, \mathbf{p} - \mathbf{q})$
- $W[P_{\mathbf{k}}\Psi](\mathbf{x}, \mathbf{p}) = W[\Psi](\mathbf{x}, \mathbf{p} - 2|\mathbf{k}|\mathbf{x})$
- $W[Q_{\mathbf{k}}\Psi](\mathbf{x}, \mathbf{p}) = W[\Psi](\mathbf{x} - \frac{\mathbf{p}}{2|\mathbf{k}|}, \mathbf{p})$

Moreover, $W[\Psi^*](\mathbf{x}, \mathbf{p}) = W[\Psi](\mathbf{x}, -\mathbf{p})$.

We note that all the above operations result in *volume-preserving* affine transformations of the phase space coordinates. Another non-trivial operator leading to a linear transformation in the phase space coordinates is the Schrödinger semigroup $e^{i\alpha\pi H/2}$ for the harmonic oscillator Hamiltonian $H = -\Delta + |\mathbf{x}|^2 - 1$. Note that H and the Fourier transform $\mathfrak{F}$ commute and share the same set of eigenfunctions, the Hermite functions (26). Indeed, $\mathfrak{F} = \exp(i\pi H/2)$. In view of the fact the Fourier transform corresponds to $\frac{\pi}{2}$-rotation in the phase plane, it is natural to define the *fractional Fourier transform* $\mathfrak{F}^\alpha$ *of order* α as the $\alpha\pi/2$ rotation:

$$W[\mathfrak{F}^\alpha\Psi](\mathbf{x}, \mathbf{p}) = W[\Psi](\mathbf{x}\cos\frac{\alpha\pi}{2} + \mathbf{p}\sin\frac{\alpha\pi}{2}, \mathbf{p}\cos\frac{\alpha\pi}{2} - \mathbf{x}\sin\frac{\alpha\pi}{2})$$

[39]. Moreover, $\mathfrak{F}^\alpha = e^{i\alpha\pi H/2}\Psi$ As a consequence of the above, the Radon transform of W at any angle in the phase plane is proportional to the square modulus of some fractional Fourier transform of Ψ and hence is non-negative pointwise. It is noteworthy that all the above transformation can be realized by simple optical systems [12]. In quantum optics, the coherent and squeezed states of light can be generated from the vacuum state, corresponding to Ψ_0 in (26), by phase space translation, rotation and sqeezing operators, all volume-preserving linear transformations.

Let us state a few more properties of the Wigner transform. If $\Psi = \Psi_1 \star \Psi_2$ where $\star$ stands for the spatial convolution then

$$W[\Psi] = \int W[\Psi_1](\mathbf{x} - \mathbf{y}, \mathbf{p})W[\Psi_2](\mathbf{y}, \mathbf{p})d\mathbf{y}$$

which is not obvious since the Wigner transform is quadratic. Likewise the pointwise product leads to the momentum convolution

$$W[\Psi_1\Psi_2] = \int W[\Psi_1](\mathbf{x}, \mathbf{p}-\mathbf{q})W[\Psi_2](\mathbf{x}, \mathbf{q})d\mathbf{q}.$$

The next property is called the Moyal identity

$$\int W[\Psi_1]W[\Psi_2]d\mathbf{x}d\mathbf{p} = \frac{1}{(2\pi)^d}\Big|\int \Psi_1\Psi_2^* d\mathbf{x}\Big|^2, \quad \forall \Psi_1, \Psi_2 \in L^2(\mathbb{R}^d).$$

The fundamental property of the Wigner distribution in application to signal analysis is this theorem [39]:

Theorem 1 *Let $\Psi_j, j \in \mathbb{N}$, be the sequence of L^2-functions and let W_j be the Wigner distribution of Ψ_j. Then the following two properties are equivalent*

$$\Psi_j, j \in \mathbb{N}, \textit{ is an orthonormal basis for } L^2 \tag{32}$$

$$\begin{cases} \sum_j W_j(\mathbf{x}, \mathbf{p}) = 1, \forall \mathbf{x}, \mathbf{p} \\ \int W_i W_j d\mathbf{x}d\mathbf{p} = \frac{\delta_{ij}}{(2\pi)^d}. \end{cases} \tag{33}$$

The first property in (33) is the partition of unity in the phase-space coordinates. The second property (33) is the consequence of the Moyal identity. As a result of the theorem, the set of Wigner distributions associated with the Hermite functions $\{\Psi_m\}$ satisfies (33), i.e. partition of unity in the phase space and the orthogonality.

The most "troublesome" feature of the Wigner distribution is its possible negative value (Fig. 15 and 16) and the resulting *lack* of uniform L^1-estimate like

$$\int \Big|W\Big| d\mathbf{x}d\mathbf{p} < C \tag{34}$$

for some constant C and all $\|\Psi\|_2 = 1$. As a result, the first property holds only in the sense of distribution. On the other hand, the Wigner distribution satisfies uniform bound in L^∞ and L^2.

Before ending this section, let us note that if $u(z, \mathbf{x})$ is governed by (14) then $W[u]$ satisfies

$$\frac{\partial}{\partial z}W + \frac{\mathbf{p}}{k} \cdot \nabla_{\mathbf{x}} W = 0.$$

which can be solved by method of characteristics.

IV. MARKOVIAN APPROXIMATION

For the weak fluctuation regime the Rytov method is suitable. The strong fluctuation regime is harder. For the statistically homogeneous random media, the Markovian model is fundamental and widely used [55].

A. White-noise scaling

We will take a somewhat different formulation in terms of the Wigner distribution. First let us non-dimensionalize the paraxial wave equation by setting

$$z \to z/L_z, \quad \mathbf{x} \to \mathbf{x}/L_x \tag{35}$$

where L_z is roughly the distance of propagation and L_x is some reference length. For example, it is natural to choose L_x as the correlation length of the index fluctuation. We obtain

$$i\frac{\partial \Psi}{\partial z} + \frac{\gamma}{2}\Delta\Psi + kL_z\tilde{n}(zL_z, \mathbf{x}L_x)\Psi = 0 \tag{36}$$

where γ is the dimensionless Fresnel number

$$\gamma = \frac{L_z}{kL_x^2}.$$

The Fraunhoffer diffraction corresponds to $\gamma \to \infty$ when, e.g. $L_z \to \infty$ with k_0, L_x fixed; the Fresnel diffraction corresponds to $\gamma = O(1)$; the geometrical optics limit corresponds to $\gamma \to 0$ when, e.g. $k_0 \to \infty$ with L_z, L_x fixed.

Note that when $k_0 \gg 1$ or $L_z \gg 1$ the fluctuation can be large even when $\tilde{n} \ll 1$. Below we shall write

$$kL_z\tilde{n}(zL_z, \mathbf{x}L_x) = \frac{\sqrt{L_z}}{\gamma}V(zL_z, \mathbf{x}).$$

The purpose of this is to introduce the normalized potential V which has $O(1)$ magnitude and transverse correlation length so that the right hand side manifests the central-limit scaling.

To study the long distance propagation $L_z \equiv \varepsilon^{-2} \to \infty$ limit while μ, γ are fixed.

For arbitrary Fresnel number we redefine the Wigner distribution as

$$W(\mathbf{x}, \mathbf{k}) = \frac{1}{(2\pi)^d}\int e^{-i\mathbf{k}\cdot\mathbf{y}}\Psi(\mathbf{x} + \frac{\gamma\mathbf{y}}{2})\Psi^*(\mathbf{x} - \frac{\gamma\mathbf{y}}{2})d\mathbf{y}. \tag{37}$$

All the nice properties of the Wigner distribution for $\gamma = 1$ survive with suitable rescaling.

The Wigner distribution satisfies an evolution equation, called the Wigner-Moyal equation,

$$\frac{\partial W}{\partial z} + \mathbf{p}\cdot\nabla_{\mathbf{x}}W + \mathcal{V}W = 0 \tag{38}$$

with the initial data

$$W_0(\mathbf{x}, \mathbf{k}) = \frac{1}{(2\pi)^d}\int e^{i\mathbf{k}\cdot\mathbf{y}}\Psi_0(\mathbf{x} - \frac{\gamma\mathbf{y}}{2})\Psi_0^*(\mathbf{x} + \frac{\gamma\mathbf{y}}{2})d\mathbf{y}\,, \tag{39}$$

where the operator $\mathcal{V}$ is formally given as

$$\mathcal{V}W \;=\; i\int e^{i\mathbf{q}\cdot\mathbf{x}}\gamma^{-1}\left[W(\mathbf{x},\mathbf{p}+\gamma\mathbf{q}/2)-W(\mathbf{x},\mathbf{p}-\gamma\mathbf{q}/2)\right]\widehat{V}(\frac{z}{\varepsilon^2},d\mathbf{q}).$$

Before taking the limit $\varepsilon\to 0$, let us pause to comment on the geometrical optics limit $\gamma\to 0$. It is not hard to show that the Wigner-Moyal equation converges formally to

$$\frac{\partial}{\partial z}W+\mathbf{p}\cdot\nabla_{\mathbf{x}}W+\nabla_{\mathbf{x}}V\cdot\nabla_{\mathbf{p}}W=0$$

which is known as the Liouville equation in classical Hamiltonian mechanics. The Liouville equation is equivalent to the Hamiltonian system with the Hamiltonian $|\mathbf{p}|^2/2+V$. Conventionally, the geometrical optics limit is approached by using the WKB method.

B. Markovian limit

Let us return to the limit with $\varepsilon\to 0$. It can be proved under very general condition that the weak solution of the Wigner-Moyal equation converges in law to the Markov process governed by the Itô equation [16]

$$dW_z \;=\; (-\mathbf{p}\cdot\nabla_{\mathbf{x}}+\mathcal{Q}_0)\,W_z\,dz+d\mathcal{B}_zW_z,\quad W_0(\mathbf{x})\in L^2(\mathbb{R}^{2d}) \tag{40}$$

or as the Stratonovich's equation

$$dW_z \;=\; -\mathbf{p}\cdot\nabla_{\mathbf{x}}+d\mathcal{B}_z\circ W_z,\quad W_0(\mathbf{x})\in L^2(\mathbb{R}^{2d})$$

where $\mathcal{B}_z$ is the operator-valued Brownian motion with the covariance operator $\mathcal{Q}$, i.e.

$$\mathbb{E}\left[d\mathcal{B}_z\theta(\mathbf{x},\mathbf{p})d\mathcal{B}_{z'}\theta(\mathbf{y},\mathbf{q})\right] \;=\; \delta(z-z')\mathcal{Q}(\theta\otimes\theta)(\mathbf{x},\mathbf{p},\mathbf{y},\mathbf{q})dzdz'.$$

Here the covariance operators $\mathcal{Q},\mathcal{Q}_0$ are defined as

$$\begin{aligned}\mathcal{Q}_0\theta \;&=\; \int\Phi(\mathbf{q})\gamma^{-2}\left[-2\theta(\mathbf{x},\mathbf{p})+\theta(\mathbf{x},\mathbf{p}-\gamma\mathbf{q})+\theta(\mathbf{x},\mathbf{p}+\gamma\mathbf{q})\right]d\mathbf{q}.\\ \mathcal{Q}(\theta\otimes\theta)(\mathbf{x},\mathbf{p},\mathbf{y},\mathbf{q}) \;&=\; \int e^{i\mathbf{q}'\cdot(\mathbf{x}-\mathbf{y})}\Phi(\mathbf{q}')\gamma^{-2}\left[\theta(\mathbf{x},\mathbf{p}-\gamma\mathbf{q}'/2)-\theta(\mathbf{x},\mathbf{p}+\gamma\mathbf{q}'/2)\right]\\ &\qquad\times\left[\theta(\mathbf{y},\mathbf{q}-\gamma\mathbf{q}'/2)-\theta(\mathbf{y},\mathbf{q}+\gamma\mathbf{q}'/2)\right]d\mathbf{q}'.\end{aligned}$$

If we take the simultaneous limit $\gamma,\epsilon\to 0$ then the covariance operators become

$$\begin{aligned}\mathcal{Q}_0\theta(\mathbf{x},\mathbf{p}) \;&=\; \nabla_{\mathbf{p}}\cdot\int\Phi(\mathbf{q})\mathbf{q}\otimes\mathbf{q}\,d\mathbf{q}\cdot\nabla_{\mathbf{p}}\theta(\mathbf{x},\mathbf{p})\\ \mathcal{Q}(\theta\otimes\theta)(\mathbf{x},\mathbf{p},\mathbf{y},\mathbf{q}) \;&=\; \nabla_{\mathbf{p}}\theta(\mathbf{x},\mathbf{p})\cdot\left[\int e^{i\mathbf{q}'\cdot(\mathbf{x}-\mathbf{y})}\Phi(\mathbf{q}')\mathbf{q}'\otimes\mathbf{q}'d\mathbf{q}'\right]\cdot\nabla_{\mathbf{q}}\theta(\mathbf{y},\mathbf{q}).\end{aligned}$$

The most useful feature of the Markovian model is that all the moments satisfy closed form equations we arrive after some algebra the following equation

$$\frac{\partial F^{(n)}}{\partial z} \;=\; -\sum_{j=1}^{n} \mathbf{p}_j \cdot \nabla_{\mathbf{x}_j} F^{(n)} + \sum_{j=1}^{n} \mathcal{Q}_0(\mathbf{x}_j, \mathbf{p}_j) F^{(n)} + \sum_{\substack{j,k=1 \\ j\neq k}}^{n} \mathcal{Q}(\mathbf{x}_j, \mathbf{p}_j, \mathbf{x}_k, \mathbf{p}_k) F^{(n)} \tag{41}$$

for the $n-$point correlation function

$$F^{(n)}(z, \mathbf{x}_1, \mathbf{p}_1, \ldots, \mathbf{x}_n, \mathbf{p}_n) \equiv \mathbb{E}\left[W_z(\mathbf{x}_1, \mathbf{p}_1) \cdots W_z(\mathbf{x}_n, \mathbf{p}_n)\right]$$

where $\mathcal{Q}_0(\mathbf{x}_j, \mathbf{p}_j)$ is the operator $\mathcal{Q}_0$ acting on the variables $(\mathbf{x}_j, \mathbf{p}_j)$ and $\mathcal{Q}(\mathbf{x}_j, \mathbf{p}_j, \mathbf{x}_k, \mathbf{p}_k)$ is the operator $\mathcal{Q}$ acting on the variables $(\mathbf{x}_j, \mathbf{p}_j, \mathbf{x}_k, \mathbf{p}_k)$.

Eq. (41) can be compactly written as

$$\frac{\partial F^{(n)}}{\partial z} \;=\; -\sum_{j=1}^{n} \mathbf{p}_j \cdot \nabla_{\mathbf{x}_j} F^{(n)} + \sum_{j,k=1}^{n} \mathcal{Q}(\mathbf{x}_j, \mathbf{p}_j, \mathbf{x}_k, \mathbf{p}_k) F^{(n)} \tag{42}$$

with the identification $\mathcal{Q}(\mathbf{x}_j, \mathbf{p}_j, \mathbf{x}_j, \mathbf{p}_j) = \mathcal{Q}_0(\mathbf{x}_j, \mathbf{p}_j)$. The operator

$$\mathcal{Q}_{\text{sum}} = \sum_{j,k=1}^{n} \mathcal{Q}(\mathbf{x}_j, \mathbf{p}_j, \mathbf{x}_k, \mathbf{p}_k) \tag{43}$$

is a non-positive symmetric operator.

In the case of the Liouville equation, eq. (42) can be more explicitly written as the Fokker-Planck equation on the phase space

$$\frac{\partial F^{(n)}}{\partial z} \;=\; \sum_{j=1}^{n} \mathbf{p}_j \cdot \nabla_{\mathbf{x}_j} F^{(n)} + \sum_{j,k=1}^{n} \mathbf{D}(\mathbf{x}_j - \mathbf{x}_k) : \nabla_{\mathbf{p}_j} \nabla_{\mathbf{p}_k} F^{(n)} \tag{44}$$

with

$$\mathbf{D}(\mathbf{x}_j - \mathbf{x}_k) \;=\; \int e^{i\mathbf{q}\cdot(\mathbf{x}_j - \mathbf{x}_k)} \Phi(\mathbf{q}) \mathbf{q} \otimes \mathbf{q} d\mathbf{q}.$$

Eq. (42) for $n = 1$ takes the following form

$$\frac{\partial}{\partial z}\bar{W} + \mathbf{p} \cdot \nabla_{\mathbf{x}} \bar{W} = \mathcal{Q}_0 \bar{W}$$

which is exactly solvable since $\mathcal{Q}_0$ is a convolution operator. The Green function is

$$\begin{aligned} G_w(z, \mathbf{x}, \mathbf{p}, \bar{\mathbf{x}}, \bar{\mathbf{p}}) \;=\; & \frac{1}{(2\pi)^2} \int \exp\left[i(\mathbf{q} \cdot (\mathbf{x} - \bar{\mathbf{x}}) - \mathbf{y} \cdot (\mathbf{p} - \bar{\mathbf{p}}) - z\mathbf{q} \cdot \bar{\mathbf{p}})\right] \\ & \times \exp\left[-\frac{1}{\gamma^2} \int_0^z D_*(\gamma \mathbf{y} + \mathbf{q}\gamma s) ds\right] d\mathbf{y} d\mathbf{q} \end{aligned} \tag{45}$$

where the (medium) structure function D_* is given by

$$D_*(\mathbf{x}) \;=\; \int \Phi(0,\mathbf{q})\left[1-e^{i\mathbf{x}\cdot\mathbf{q}}\right]\,d\mathbf{q}. \tag{46}$$

We shall refer to $\exp\left[-\gamma^{-2}\int_0^z D_*(\gamma\mathbf{y}+\mathbf{q}\gamma s)ds\right]$ as the *wave* structure function. The case $n=2$ can be approximately solved in certain circumstances. In the next section, we discuss the application of these equations to the time reversal of waves in random media.

The most important quantity for us is the mutual coherence function $\Gamma_2(z,\mathbf{x}_1,\mathbf{x}_2;\bar{\mathbf{x}}_1,\bar{\mathbf{x}}_2) = \mathbb{E}\Big[\Psi_1(z,\mathbf{x}_1)\Psi_2(z,\mathbf{x}_2)\Big]$ with $\Psi_1(0,\mathbf{x}_1)=\delta(\mathbf{x}_1-\bar{\mathbf{x}}_1)$ and $\Psi_2(0,\mathbf{x}_1)=\delta(\mathbf{x}_1-\bar{\mathbf{x}}_2)$. From (37) it follows that

$$\bar{W}(0,\mathbf{x},\mathbf{p}) = \frac{1}{(2\pi)^2}e^{\frac{i}{\gamma}(\bar{\mathbf{x}}_2-\bar{\mathbf{x}}_1)\cdot\mathbf{p}}\delta(2\mathbf{x}-\bar{\mathbf{x}}_1-\bar{\mathbf{x}}_2)$$

which then yields by (45)

$$\bar{W}(z,\mathbf{x},\mathbf{p}) = \frac{1}{(2\pi)^2}\int e^{i\mathbf{q}\cdot\left(\mathbf{x}-\frac{\bar{\mathbf{x}}_1+\bar{\mathbf{x}}_2}{2}\right)}e^{i\left(\frac{\bar{\mathbf{x}}_2-\bar{\mathbf{x}}_1}{\gamma}-z\mathbf{q}\right)\cdot\mathbf{p}}e^{-\frac{1}{\gamma^2}\int_0^z D_*(\bar{\mathbf{x}}_2-\bar{\mathbf{x}}_1-\mathbf{q}\gamma s)ds}d\mathbf{q}$$

By (31) we have

$$\Gamma_2(z,\mathbf{x}_1,\mathbf{x}_2;\bar{\mathbf{x}}_1,\bar{\mathbf{x}}_2) \;=\; \int \bar{W}(z,\frac{1}{2}(\mathbf{x}_1+\mathbf{x}_2),\mathbf{p})\exp\left[i\mathbf{p}\cdot(\mathbf{x}_1-\mathbf{x}_2)/\gamma\right]d\mathbf{p}.$$

and hence

$$\Gamma_2(z,\mathbf{x}_1,\mathbf{x}_2;\bar{\mathbf{x}}_1,\bar{\mathbf{x}}_2) \;=\; \frac{1}{z^2}e^{\frac{i}{2z\gamma}\left(\mathbf{x}_1-\mathbf{x}_2-\bar{\mathbf{x}}_1+\bar{\mathbf{x}}_2\right)\cdot\left(\mathbf{x}_1+\mathbf{x}_2-\bar{\mathbf{x}}_1-\bar{\mathbf{x}}_2\right)}e^{-\frac{z}{\gamma^2}\int_0^1 D_*((1-s)(\bar{\mathbf{x}}_2-\bar{\mathbf{x}}_1)+s(\mathbf{x}_2-\mathbf{x}_1))ds} \tag{47}$$

V. TWO-FREQUENCY TRANSPORT THEORY

When the wavelength is comparable to the spatial scale of medium fluctuations then a different scaling and approximation, called radiative transfer, is valid.

Instead of the standard one-frequency transport theory, we will present the two-frequency formulation and deduce the one-frequency theory as a special case.

A. paraxial waves

Analysis of pulsed signal propagation in random media often requires spectral decomposition of the time-dependent signal and the correlation information of two different frequency components. In the conventional approach, the analysis is in terms of the two-frequency mutual coherence function

$$\Gamma_{12}(z,\mathbf{x},\mathbf{y}) = \mathbb{E}[\Psi_1(z,\mathbf{x}+\frac{\gamma\mathbf{y}}{2})\Psi_2(z,\mathbf{x}-\frac{\gamma\mathbf{y}}{2})]$$

and uses various ad hoc approximations [38].

Let k_1, k_2 be two (relative) wavenumbers nondimensionlized by the central wavenumber k_0. We write the paraxial wave equation in the dimensionless form

$$i\frac{\partial}{\partial z}\Psi_j(z,\mathbf{x}) + \frac{\gamma}{2k_j}\nabla^2\Psi_j(z,\mathbf{x}) + \frac{\mu k_j}{\gamma}V(\frac{z}{\varepsilon^2},\frac{\mathbf{x}}{\varepsilon^{2\alpha}})\Psi_j(z,\mathbf{x}) = 0, \quad j = 1,2 \tag{48}$$

where γ is the Fresnel number w.r.t. the central wavenumber.

An important regime for classical wave propagation takes place when the transverse correlation length is much smaller than the propagation distance but is comparable or much larger than the central wavelength which is proportional to the Fresnel number. This is the radiative transfer regime for monochromatic waves described by the following scaling limit

$$\gamma = \theta\varepsilon^{2\alpha}, \quad \mu = \varepsilon^{2\alpha-1}, \quad \theta > 0, \quad \text{such that} \quad \lim_{\varepsilon\to 0}\theta < \infty, \tag{49}$$

(see [15], [22] and references therein). With two different frequencies, the most interesting scaling limit requires another simultaneous limit

$$\lim_{\varepsilon\to 0} k_1 = \lim_{\varepsilon\to 0} k_2 = k, \quad \lim_{\varepsilon\to 0}\gamma^{-1}k^{-1}(k_2 - k_1) = \beta > 0. \tag{50}$$

We shall refer to the conditions (49) and (50) as the two-frequency radiative transfer scaling limit.

But in the radiative transfer regime the two-frequency mutual coherence function is not as convenient as the two-frequency Wigner distribution, introduced in [17], which is a natural extension of the standard Wigner distribution and is self-averaging in the radiative transfer regime.

The two-frequency Wigner distribution is defined as

$$W_z(\mathbf{x},\mathbf{p}) = \frac{1}{(2\pi)^d}\int e^{-i\mathbf{p}\cdot\mathbf{y}}\Psi_1(z,\frac{\mathbf{x}}{\sqrt{k_1}} + \frac{\gamma\mathbf{y}}{2\sqrt{k_1}})\Psi_2^*(z,\frac{\mathbf{x}}{\sqrt{k_2}} - \frac{\gamma\mathbf{y}}{2\sqrt{k_2}})d\mathbf{y} \tag{51}$$

where the scaling factor $\sqrt{k_j}$ is introduced so that W_z satisfies a closed-form equation (see below).

The following property can be derived easily from the definition

$$\|W_z\|_2 \;=\; \left(\frac{\sqrt{k_1k_2}}{2\gamma\pi}\right)^{d/2}\|\Psi_1(z,\cdot)\|_2\|\Psi_2(z,\cdot)\|_2.$$

Hence the L^2-norm is conserved $\|W_z\|_2 = \|W_0\|_2$. The Wigner distribution has the following obvious properties:

$$\int W_z(\mathbf{x},\mathbf{p})e^{i\mathbf{p}\cdot\mathbf{y}}d\mathbf{p} \;=\; \Psi_1(z,\frac{\mathbf{x}}{\sqrt{k_1}} + \frac{\gamma\mathbf{y}}{2\sqrt{k_1}})\Psi_2^*(z,\frac{\mathbf{x}}{\sqrt{k_2}} - \frac{\gamma\mathbf{y}}{2\sqrt{k_2}}) \tag{52}$$

$$\int_{\mathbb{R}^d} W_z(\mathbf{x},\mathbf{p})e^{-i\mathbf{x}\cdot\mathbf{q}}d\mathbf{x} \;=\; \left(\frac{\pi^2\sqrt{k_1k_2}}{\gamma}\right)^d \widehat{\Psi}_1(z,\frac{\mathbf{p}\sqrt{k_1}}{4\gamma} + \frac{\sqrt{k_1}\mathbf{q}}{2})\widehat{\Psi}_2^*(z,\frac{\mathbf{p}\sqrt{k_2}}{4\gamma} - \frac{\sqrt{k_2}\mathbf{q}}{2}) \tag{53}$$

and so contains essentially all the information in the two-point two-frequency function.

The Wigner distribution W_z satisfies the Wigner-Moyal equation exactly [17]

$$\frac{\partial W_z^\varepsilon}{\partial z} + \mathbf{p}\cdot\nabla_{\mathbf{x}} W_z^\varepsilon + \frac{1}{\varepsilon}\mathcal{L}_z W_z^\varepsilon = 0 \tag{54}$$

where the operator $\mathcal{L}_z$ is formally given as

$$\mathcal{L}_z W_z \;=\; i\int \theta^{-1}\left[e^{i\mathbf{q}\cdot\tilde{\mathbf{x}}/\sqrt{k_1}}k_1 W_z^\varepsilon(\mathbf{x},\mathbf{p}+\frac{\theta\mathbf{q}}{2\sqrt{k_1}}) - e^{i\mathbf{q}\cdot\tilde{\mathbf{x}}/\sqrt{k_2}}k_2 W_z^\varepsilon(\mathbf{x},\mathbf{p}-\frac{\theta\mathbf{q}}{2\sqrt{k_2}})\right]\widehat{V}(\frac{z}{\varepsilon^2},d\mathbf{q})$$

with $\tilde{\mathbf{x}} = \mathbf{x}/\varepsilon^{2\alpha}$ being the 'fast' transverse variable.

1. Two-frequency radiative transfer equations

Under the same assumptions as in the one-frequency theory [15, 22], one can show the convergence to one of the two types of transport equations as ε tends to zero.

In the first case, let $\theta > 0$ be fixed. The limit equation is

$$\frac{\partial}{\partial z}\bar{W} + \mathbf{p}\cdot\nabla\bar{W} \;=\; \frac{2\pi k^2}{\theta^2}\int K(\mathbf{p},\mathbf{q})\left[e^{-i\beta\theta\mathbf{q}\cdot\mathbf{x}/(2\sqrt{k})}\bar{W}(\mathbf{x},\mathbf{p}+\frac{\theta\mathbf{q}}{\sqrt{k}}) - \bar{W}(\mathbf{x},\mathbf{p})\right]d\mathbf{q} \tag{55}$$

where the kernel K is given by

$$K(\mathbf{p},\mathbf{q}) \;=\; \Phi(0,\mathbf{q}), \quad \text{for} \quad \alpha\in(0,1),$$

and

$$K(\mathbf{p},\mathbf{q}) \;=\; \Phi\big((\mathbf{p}+\frac{\theta\mathbf{q}}{2\sqrt{k}})\cdot\mathbf{q},\mathbf{q}\big), \quad \text{for} \quad \alpha = 1.$$

For $\alpha > 1$, then with the choice of $\mu = \varepsilon^\alpha$ the limit kernel becomes

$$K(\mathbf{p},\mathbf{q}) \;=\; \delta\big((\mathbf{p}+\frac{\theta\mathbf{q}}{2\sqrt{k}})\cdot\mathbf{q}\big)\int\Phi(w,\mathbf{q})dw.$$

In the second case, let $\lim_{\varepsilon\to 0}\theta = 0$. The limit equation becomes

$$\frac{\partial}{\partial z}W_z + \mathbf{p}\cdot\nabla W_z = k\left(\nabla_{\mathbf{p}} - \frac{i}{2}\beta\mathbf{x}\right)\cdot\mathbf{D}\cdot\left(\nabla_{\mathbf{p}} - \frac{i}{2}\beta\mathbf{x}\right)W_z \tag{56}$$

where the (momentum) diffusion coefficient $\mathbf{D}$ is given by

$$\mathbf{D} \;=\; \pi\int\Phi(0,\mathbf{q})\mathbf{q}\otimes\mathbf{q}d\mathbf{q}, \quad \text{for} \quad \alpha\in(0,1), \tag{57}$$

$$\mathbf{D}(\mathbf{p}) \;=\; \pi\int\Phi(\mathbf{p}\cdot\mathbf{q},\mathbf{q})\mathbf{q}\otimes\mathbf{q}d\mathbf{q}, \quad \text{for} \quad \alpha = 1. \tag{58}$$

For $\alpha > 1$, then with the choice of $\mu = \varepsilon^\alpha$ the limit coefficients become

$$\mathbf{D}(\mathbf{p}) \;=\; \pi|\mathbf{p}|^{-1} \int_{\mathbf{p}\cdot\mathbf{p}_\perp=0} \int \Phi(w, \mathbf{p}_\perp) dw \; \mathbf{p}_\perp \otimes \mathbf{p}_\perp d\mathbf{p}_\perp. \tag{59}$$

When $k_1 = k_2$ or $\beta = 0$, eq. (55) and (56) reduce to the standard radiative transfer equations derived in [15].

2. The longitudinal and transverse cases

To illustrate the utility of these equations, we proceed to discuss the two special cases for the transverse dimension $d = 2$. For simplicity, we will assume the isotropy of the medium in the transverse coordinates such that $\Phi(w, \mathbf{p}) = \Phi(w, |\mathbf{p}|)$. As a consequence the momentum diffusion coefficient is a scalar. In the longitudinal case $\mathbf{D} = D\mathbf{I}$ with a constant scalar D whereas in the transverse case $\mathbf{D}(\mathbf{p}) = C|\mathbf{p}|^{-1}\hat{\mathbf{p}}_\perp \otimes \hat{\mathbf{p}}_\perp$ with the constant C given by

$$C = \frac{\pi}{2} \int \int \Phi(w, \mathbf{p}_\perp) dw |\mathbf{p}_\perp|^2 d\mathbf{p}_\perp.$$

Here $\hat{\mathbf{p}}_\perp \in \mathbb{R}^2$ is an unit vector normal to $\mathbf{p} \in \mathbb{R}^2$.

First of all, the equation (56) by itself gives qualitative information about three important parameters of the stochastic channel: the spatial spread σ_*, the coherence length ℓ_c and the coherence bandwidth β_c, through the following scaling argument. One seeks the change of variables

$$\tilde{\mathbf{x}} = \frac{\mathbf{x}}{\sigma_* \sqrt{k}}, \quad \tilde{\mathbf{p}} = \mathbf{p}\ell_c\sqrt{k}, \quad \tilde{z} = \frac{z}{L}, \quad \tilde{\beta} = \frac{\beta}{\beta_c} \tag{60}$$

where L is the propagation distance to remove all the physical parameters from (56) and to aim for the form

$$\frac{\partial}{\partial \tilde{z}} W + \tilde{\mathbf{p}} \cdot \nabla_{\tilde{\mathbf{x}}} W = \left(\nabla_{\tilde{\mathbf{p}}} + \frac{i\tilde{\beta}}{2} \tilde{\mathbf{x}} \right) \cdot \left(\nabla_{\tilde{\mathbf{p}}} + \frac{i\tilde{\beta}}{2} \tilde{\mathbf{x}} \right) W \tag{61}$$

in the longitudinal case and the form

$$\frac{\partial}{\partial \tilde{z}} W + \tilde{\mathbf{p}} \cdot \nabla_{\tilde{\mathbf{x}}} W = \left(\nabla_{\tilde{\mathbf{p}}} + \frac{i\tilde{\beta}}{2} \tilde{\mathbf{x}} \right) \cdot \frac{\hat{\mathbf{p}}_\perp \otimes \hat{\mathbf{p}}_\perp}{|\tilde{\mathbf{p}}|} \cdot \left(\nabla_{\tilde{\mathbf{p}}} + \frac{i\tilde{\beta}}{2} \tilde{\mathbf{x}} \right) W \tag{62}$$

in the transverse case. From the left side of (56) it immediately follows the first duality relation $\ell_c \sigma_* \sim L/k$. The balance of terms inside each pair of parentheses leads to the second duality relation $\beta_c \sim \ell_c/\sigma_*$. Finally the removal of D or C determines the spatial

spread σ_* which has a different expression in the longitudinal and transverse case. In the longitudinal case,

$$\sigma_* \sim D^{1/2}L^{3/2}, \quad \ell_c \sim k^{-1}D^{-1/2}L^{-1/2}, \quad \beta_c \sim k^{-1}D^{-1}L^{-2}$$

whereas in the transverse case

$$\sigma_* \sim k^{-1/6}C^{1/3}L^{4/3}, \quad \ell_c \sim k^{-5/6}C^{-1}L^{-1}, \quad \ell_c \sim \beta_c \sim k^{-2/3}C^{-2/3}L^{-5/3}.$$

In the longitudinal case, the inverse Fourier transform in $\tilde{\mathbf{p}}$ renders eq. (61) to the form

$$\frac{\partial \tilde{W}}{\partial \tilde{z}} - i\nabla_{\tilde{\mathbf{y}}} \cdot \nabla_{\tilde{\mathbf{x}}} \tilde{W} \;=\; -\big|\tilde{\mathbf{y}} - \frac{\tilde{\beta}}{2}\tilde{\mathbf{x}}\big|^2 \tilde{W} \tag{63}$$

which can be solved exactly and whose Green function at $\tilde{z} = 1$ is

$$\begin{aligned}
&\frac{(1+i)^{d/2}\tilde{\beta}^{d/4}}{(2\pi)^d \sin^{d/2}\left[\tilde{\beta}^{1/2}(1+i)\right]} \exp\Big[i\frac{|\tilde{\mathbf{y}}-\mathbf{y}'|^2}{2\tilde{\beta}}\Big] \exp\Big[i\frac{(\tilde{\mathbf{y}}-\mathbf{y}')\cdot(\tilde{\mathbf{x}}-\mathbf{x}')}{2}\Big] \exp\Big[i\frac{\tilde{\beta}|\tilde{\mathbf{x}}-\mathbf{x}'|^2}{8}\Big] \\
&\times \exp\Big[\frac{1-i}{2\tilde{\beta}^{1/2}} \cot\left(\tilde{\beta}^{1/2}(1+i)\right)\big|\tilde{\mathbf{y}} - \tilde{\beta}\tilde{\mathbf{x}}/2 - \frac{\mathbf{y}' - \tilde{\beta}\mathbf{x}'/2}{\cos\left(\tilde{\beta}^{1/2}(1+i)\right)}\big|^2\Big] \\
&\times \exp\Big[-\frac{1-i}{2\tilde{\beta}^{1/2}}\Big|\mathbf{y}' - \tilde{\beta}\mathbf{x}'/2\Big|^2 \tan\left(\tilde{\beta}^{1/2}(1+i)\right)\Big],
\end{aligned} \tag{64}$$

[19]. This solution gives asymptotically precise information about the cross-frequency correlation, important for analyzing the information transfer and time reversal with broadband signals in the channel described by the random Schrödinger equation [19]. It is unclear if the transverse case is exactly solvable or not.

B. Spherical waves

The two-frequency radiative transfer theory can be extended to the spherical scalar wave as follows [21].

Let $U_j, j = 1, 2$ be governed by the reduced wave equation

$$\Delta U_j(\mathbf{r}) + k_j^2\big(\nu_j + V_j(\mathbf{r})\big)U_j(\mathbf{r}) = f_j(\mathbf{r}), \quad \mathbf{r} \in \mathbb{R}^3, \quad j = 1, 2 \tag{65}$$

where ν_j and V_j are respectively the mean and fluctuation of the refractive index associated with the wavenumber k_j and are in general complex-valued. The source terms f_j may result from the initial data or the external sources. Here and below the vacuum phase speed is set to be unity. To solve (65) one needs also some boundary condition which is assumed to be vanishing at the far field.

Radiative transfer regime is characterized by the scaling limit which replaces $\nu_j + V_j$ in eq. (65) with

$$\frac{1}{\theta^2\varepsilon^2}\Big(\nu_j + \sqrt{\varepsilon}V_j(\frac{\mathbf{r}}{\varepsilon})\Big), \quad \theta > 0, \quad \varepsilon \ll 1 \tag{66}$$

where ε is the ratio of the scale of medium fluctuation to the $O(1)$ propagation distance and θ the ratio of the wavelength to the scale of medium fluctuation.

Anticipating small-scale fluctuation due to (66) we define the two-frequency Wigner distribution in the following way

$$W(\mathbf{x},\mathbf{p}) = \frac{1}{(2\pi)^3}\int e^{-i\mathbf{p}\cdot\mathbf{y}} U_1(\frac{\mathbf{x}}{k_1}+\frac{\theta\varepsilon\mathbf{y}}{2k_1})U_2^*(\frac{\mathbf{x}}{k_2}-\frac{\theta\varepsilon\mathbf{y}}{2k_2})d\mathbf{y}$$

which satisfies the exact equation

$$\mathbf{p}\cdot\nabla W - F \;=\; \frac{i}{2\varepsilon\theta}(\nu_1-\nu_2^*)W + \frac{1}{\sqrt{\varepsilon}}\mathcal{L}W \tag{67}$$

where the operator $\mathcal{L}$ is defined as

$$\mathcal{L}W(\mathbf{x},\mathbf{p}) \;=\; \frac{i}{2\theta}\int \hat{V}_1(d\mathbf{q})e^{i\frac{\mathbf{q}\cdot\mathbf{x}}{\varepsilon k_1}}W(\mathbf{x},\mathbf{p}-\frac{\theta\mathbf{q}}{2k_1}) - \frac{i}{2\theta}\int \hat{V}_2^*(d\mathbf{q})e^{-i\frac{\mathbf{q}\cdot\mathbf{x}}{\varepsilon k_2}}W(\mathbf{x},\mathbf{p}-\frac{\theta\mathbf{q}}{2k_2})$$

and the function

$$\begin{aligned} F \;=\; & -\frac{i}{2(2\pi)^3}\int e^{-i\mathbf{p}\cdot\mathbf{y}} f_1(\frac{\mathbf{x}}{k_1}+\frac{\mathbf{y}}{2k_1})U_2^*(\frac{\mathbf{x}}{k_2}-\frac{\mathbf{y}}{2k_2})d\mathbf{y} \\ & +\frac{i}{2(2\pi)^3}\int e^{-i\mathbf{p}\cdot\mathbf{y}} U_1(\frac{\mathbf{x}}{k_1}+\frac{\mathbf{y}}{2k_1})f_2^*(\frac{\mathbf{x}}{k_2}-\frac{\mathbf{y}}{2k_2})d\mathbf{y} \end{aligned} \tag{68}$$

depends linearly on U_1 and U_2.

To capture the cross-frequency correlation in the radiative transfer regime we also need to restrict the frequency difference range

$$\lim_{\varepsilon\to 0}k_1 = \lim_{\varepsilon\to 0}k_2 = k, \quad \frac{k_2-k_1}{\varepsilon\theta k} = \beta \tag{69}$$

where $k,\beta > 0$ are independent of ε and θ. Assuming the differentiability of the mean refractive index's dependence on the wavenumber we write

$$\frac{\nu_2^*-\nu_1}{2\varepsilon\theta} = \nu' \tag{70}$$

where ν' is independent of ε,θ.

Using the multi-scale expansion we derive the two-frequency radiative transfer equation for the averaged Wigner distribution $\bar{W}$

$$\begin{aligned} & \mathbf{p}\cdot\nabla_{\mathbf{x}}\bar{W} + i\nu'\bar{W} - \mathbb{E}F \\ & = \frac{\pi k^3}{\theta^4}\int d\mathbf{q}\Phi\big(\frac{k}{\theta}(\mathbf{p}-\mathbf{q})\big)\delta(|\mathbf{p}|^2-|\mathbf{q}|^2)\Big[e^{i\mathbf{x}\cdot(\mathbf{p}-\mathbf{q})\beta}\bar{W}\big(\mathbf{x},\mathbf{q}\big)-\bar{W}(\mathbf{x},\mathbf{p})\Big]. \end{aligned} \tag{71}$$

The δ-function in the scattering kernel is due to elastic scattering which preserve the wavenumber. When $\beta = 0$ (then $\nu_1 = \nu_2$ and $i\nu' \sim$ the imaginary part of ν), eq. (71) reduce to the standard form of radiative transfer equation for the phase space energy density [7, 46]. For $\beta > 0$, the wave featue is retained in (71). When $\beta \to \infty$, the first term in the bracket on the right hand side of (71) drops out, due to rapid phase fluctuation, so the random scattering effect is pure damping:

$$\mathbf{p} \cdot \nabla_{\mathbf{x}} \bar{W} + i\nu' \bar{W} - \mathbb{E}F \;=\; -\frac{\pi k^3}{\theta^4} \int d\mathbf{q} \Phi\big(\frac{k}{\theta}(\mathbf{p} - \mathbf{q})\big) \delta(|\mathbf{p}|^2 - |\mathbf{q}|^2) \bar{W}(\mathbf{x}, \mathbf{p}).$$

1. Geometrical radiative transfer

Let us consider the further limit $\theta \ll 1$ when the wavelength is much shorter than the correlation length of the medium fluctuation. To this end, the following form is more convenient to work with

$$\begin{aligned} &\mathbf{p} \cdot \nabla_{\mathbf{x}} \bar{W} + i\nu' \bar{W} - \mathbb{E}F \\ &= \frac{\pi k}{2\theta^2} \int d\mathbf{q} \Phi\big(\mathbf{q}\big) \delta\big(\mathbf{q} \cdot (\mathbf{p} - \frac{\theta \mathbf{q}}{2k})\big) \Big[e^{i\mathbf{x}\cdot\mathbf{q}\beta\theta/k} \bar{W}\big(\mathbf{x}, \mathbf{p} - \frac{\theta \mathbf{q}}{k}\big) - \bar{W}(\mathbf{x}, \mathbf{p}) \Big] \end{aligned} \tag{72}$$

which is obtained from eq. (71) after a change of variables. We expand the right hand side of (72) in θ and pass to the limit $\theta \to 0$ to obtain

$$\mathbf{p} \cdot \nabla_{\mathbf{x}} \bar{W} + i\nu' \bar{W} - \mathbb{E}F \;=\; \frac{1}{4k} \left(\nabla_{\mathbf{p}} - i\beta \mathbf{x}\right) \cdot \mathbf{D} \cdot \left(\nabla_{\mathbf{p}} - i\beta \mathbf{x}\right) \bar{W} \tag{73}$$

with the (momentum) diffusion coefficient

$$\mathbf{D}(\mathbf{p}) = \pi \int \Phi(\mathbf{q}) \delta(\mathbf{p} \cdot \mathbf{q}) \mathbf{q} \otimes \mathbf{q} d\mathbf{q}. \tag{74}$$

The symmetry $\Phi(\mathbf{p}) = \Phi(-\mathbf{p})$ plays an explicit role here in rendering the right hand side of eq. (72) a second-order operator in the limit $\theta \to 0$. Eq. (73) can be rigorously derived from geometrical optics by a probabilistic method [20].

2. Spatial (frequency) spread and coherence bandwidth

Through dimensional analysis, eq. (73) yields qualitative information about important physical parameters of the stochastic medium. To show this, let us assume for simplicity the isotropy of the medium, i.e. $\Phi(\mathbf{p}) = \Phi(|\mathbf{p}|)$, so that $\mathbf{D} = C|\mathbf{p}|^{-1}\Pi(\mathbf{p})$ where

$$C = \frac{\pi}{3} \int \delta\Big(\frac{\mathbf{p}}{|\mathbf{p}|} \cdot \frac{\mathbf{q}}{|\mathbf{q}|}\Big) \Phi(|\mathbf{q}|) |\mathbf{q}| d\mathbf{q} \tag{75}$$

is a constant and $\Pi(\mathbf{p})$ the orthogonal projection onto the plane perpendicular to $\mathbf{p}$. In view of (73) C (and $\mathbf{D}$) has the dimension of inverse length while the variables $\mathbf{x}$ and $\mathbf{p}$ are dimensionless.

Now consider the following change of variables

$$\mathbf{x} = \sigma_x k \tilde{\mathbf{x}}, \quad \mathbf{p} = \sigma_p \tilde{\mathbf{p}}/k, \quad \beta = \beta_c \tilde{\beta} \tag{76}$$

where σ_x and σ_p are respectively the spreads in position and spatial frequency, and β_c is the coherence bandwidth. Let us substitute (76) into eq. (73) and aim for the standard form

$$\tilde{\mathbf{p}} \cdot \nabla_{\tilde{\mathbf{x}}} \bar{W} + i\nu' \bar{W} - \langle F \rangle \;=\; \left(\nabla_{\tilde{\mathbf{p}}} - i\tilde{\beta}\tilde{\mathbf{x}} \right) \cdot |\tilde{\mathbf{p}}|^{-1} \Pi(\tilde{\mathbf{p}}) \left(\nabla_{\tilde{\mathbf{p}}} - i\tilde{\beta}\tilde{\mathbf{x}} \right) \bar{W}. \tag{77}$$

The 1-st term on the left side yields the first duality relation

$$\sigma_x / \sigma_p \sim 1/k^2. \tag{78}$$

The balance of terms in each pair of parentheses yields the second duality relation

$$\sigma_x \sigma_p \sim \frac{1}{\beta_c} \tag{79}$$

whose left hand side is the *space-spread-bandwidth product.* Finally the removal of the constant C determines

$$\sigma_p \sim k^{2/3} C^{1/3} \tag{80}$$

from which σ_x and β_c can be determined by using (78) and (79):

$$\sigma_x \sim k^{-4/3} C^{1/3}, \quad \beta_c \sim k^{2/3} C^{-2/3}.$$

We do not know if, as it stands, eq. (77) is analytically solvable but we can solve analytically for its boundary layer behavior.

3. Small-scale asymptotics

Consider the propagation distance less than the transport mean-free-path. The corresponding two-frequency Wigner distribution would be highly concentrated at the longitudinal momentum, say, $p = 1$. Hence we can assume that the projection $\Pi(\mathbf{p})$ in (77) is effectively just the projection onto the transverse plane coordinated by $\mathbf{x}_\perp$ and approximate eq. (73) by

$$\left[\partial_z + \mathbf{p}_\perp \cdot \nabla_{\mathbf{x}_\perp} \right] \bar{W} + i\nu' \bar{W} - \mathbb{E}F \;=\; \frac{C_\perp}{4k|p|} \left(\nabla_{\mathbf{p}_\perp} - i\beta \mathbf{x}_\perp \right)^2 \bar{W} \tag{81}$$

where the constant $C_\perp$ is the paraxial approximation of (74) for $|p| = 1$:

$$C_\perp = \frac{\pi}{2} \int \Phi(0, \mathbf{q}_\perp) |\mathbf{q}_\perp|^2 d\mathbf{q}_\perp.$$

Note that the longitudinal (momentum) diffusion vanishes and that the longitudinal momentum p plays the role of a parameter in eq. (81) which then can be solved in the direction of increasing z as an evolution equation with initial data given at a fixed z.

Let σ_* be the spatial spread in the transverse coordinates $\mathbf{x}_\perp$, ℓ_c the coherence length in the transverse dimensions and β_c the coherence bandwidth. Let L be the scale of the boundary layer. We then seek the following change of variables

$$\tilde{\mathbf{x}}_\perp = \frac{\mathbf{x}_\perp}{\sigma_* k}, \quad \tilde{\mathbf{p}}_\perp = \mathbf{p}_\perp k \ell_c, \quad \tilde{z} = \frac{z}{Lk}, \quad \tilde{\beta} = \frac{\beta}{\beta_c} \tag{82}$$

to remove all the physical parameters from (81) and to aim for the form

$$\partial_{\tilde{z}} \bar{W} + \tilde{\mathbf{p}}_\perp \cdot \nabla_{\tilde{\mathbf{x}}_\perp} \bar{W} + Lki\nu' \bar{W} - Lk\mathbb{E}F = \left(\nabla_{\tilde{\mathbf{p}}_\perp} - i\tilde{\beta} \tilde{\mathbf{x}}_\perp \right)^2 \bar{W}. \tag{83}$$

The same reasoning as above now leads to

$$\ell_c \sigma_* \sim L/k, \quad \sigma_*/\ell_c \sim 1/\beta_c, \quad \ell_c \sim k^{-1} L^{-1/2} C_\perp^{-1/2}$$

and hence

$$\sigma_* \sim L^{3/2} C_\perp^{1/2}, \quad \beta_c \sim k^{-1} C_\perp^{-1} L^{-2}.$$

The layer thickness L may be determined by $\ell_c \sim 1$, i.e. $L \sim k^{-2} C_\perp^{-1}$.

After the inverse Fourier transform eq. (83) becomes

$$\partial_{\tilde{z}} \Gamma - i \nabla_{\tilde{\mathbf{y}}_\perp} \cdot \nabla_{\tilde{\mathbf{x}}_\perp} \Gamma + Lki\nu' \Gamma - Lk\mathbb{E}F \; = \; - \left| \tilde{\mathbf{y}}_\perp + \tilde{\beta} \tilde{\mathbf{x}}_\perp \right|^2 \Gamma \tag{84}$$

which is the governing equation for the two-frequency mutual coherence in the normalized variables. With data given on $\tilde{z} = 0$ and vanishing far-field boundary condition in the transverse directions, Eq. (84) can be solved analytically and its Green function is analogous to (64):

$$\begin{aligned} &\frac{e^{-iLk\nu'} (i4\tilde{\beta})^{1/2}}{(2\pi)^2 \tilde{z} \sinh\left[(i4\tilde{\beta})^{1/2} \tilde{z}\right]} \exp\left[\frac{1}{i4\tilde{\beta}\tilde{z}} \left| \tilde{\mathbf{y}}_\perp - \tilde{\beta}\tilde{\mathbf{x}}_\perp - \mathbf{y}'_\perp + \tilde{\beta}\mathbf{x}'_\perp \right|^2 \right] \\ &\times \exp\left[-\frac{\coth\left[(i4\tilde{\beta})^{1/2}\tilde{z}\right]}{(i4\tilde{\beta})^{1/2}} \left| \tilde{\mathbf{y}}_\perp + \tilde{\beta}\tilde{\mathbf{x}}_\perp - \frac{\mathbf{y}'_\perp + \tilde{\beta}\mathbf{x}'_\perp}{\cosh\left[(i4\tilde{\beta})^{1/2}\tilde{z}\right]} \right|^2 \right] \\ &\times \exp\left[-\frac{\tanh\left[(i4\tilde{\beta})^{1/2}\tilde{z}\right]}{(i4\tilde{\beta})^{1/2}} \left| \mathbf{y}'_\perp + \tilde{\beta}\mathbf{x}'_\perp \right|^2 \right]. \end{aligned} \tag{85}$$

VI. APPLICATION: TIME REVERSAL

Time reversal is the process of recording the signal from a remote source, time-reversing and back-propagating it to retrofocus around the source. Time reversal of acoustic waves has been demonstrated to hold exciting technological potentials in subwavelength focusing, dispersion compensation, communications, imaging, remote-sensing and target detection in unknown environments (see [29], [30], [41] and references therein). The same should hold for the electromagnetic waves as well. Time reversal of electromagnetic waves is closely related to optical phase conjugation [34].

A. Spherical wave

In the simplest version of time reversal, a compactly supported, monochromatic source f emits a wave field u which is then recorded at the boundary ∂D enclosing the support of f. u satisfies the inhomogeneous Helmholtz equation

$$\Delta u + k^2 u = f.$$

Suppose both u and $\partial u/\partial n$ are recorded at ∂D, phase-conjugated and back-propagated into the domain D by using, respectively, $\partial G_0/\partial n$ and G_0. For a monochromatic wave, phase conjugation is equivalent to time reversal. We obtain as a result

$$v(\mathbf{r}) \equiv \int_{\partial D} u^*(\mathbf{r}') \frac{\partial G_0(\mathbf{r}-\mathbf{r}')}{\partial n} d\sigma(\mathbf{r}') - \int_{\partial D} \frac{\partial u^*(\mathbf{r}')}{\partial n} G_0(\mathbf{r}-\mathbf{r}') d\sigma(\mathbf{r}'). \tag{86}$$

Clearly, $v(\mathbf{r})$ is a solution of the homogeneous Helmholtz equation.

By the second Green identity

$$\begin{aligned} &\int_{\partial D} u^*(\mathbf{r}') \frac{\partial G_0(\mathbf{r}-\mathbf{r}')}{\partial n} d\sigma(\mathbf{r}') - \int_{\partial D} \frac{\partial u^*(\mathbf{r}')}{\partial n} G_0(\mathbf{r}-\mathbf{r}') d\sigma(\mathbf{r}') \\ = &\int_D u^*(\mathbf{r}')(\Delta + k^2) G(\mathbf{r}-\mathbf{r}') d\mathbf{r}' - \int_D (\Delta + k^2) u^*(\mathbf{r}') G_0(\mathbf{r}-\mathbf{r}') d\mathbf{r}' \end{aligned} \tag{87}$$

we have

$$v(\mathbf{r}) \;=\; u^*(\mathbf{r}) - \int_D f^*(\mathbf{r}') G_0(\mathbf{r}-\mathbf{r}') d\mathbf{r}'.$$

Therefore

$$\begin{aligned} v(\mathbf{r}) \;&=\; \int_D G_0^*(\mathbf{r}-\mathbf{r}') f(\mathbf{r}') d\mathbf{r}' - \int_D G_0(\mathbf{r}-\mathbf{r}') f^*(\mathbf{r}') d\mathbf{r}' \\ &=\; \int_D \left[G_0^*(\mathbf{r}-\mathbf{r}') - G_0(\mathbf{r}-\mathbf{r}') \right] f^*(\mathbf{r}') d\mathbf{r}' \\ &=\; \frac{1}{2\pi i} \int_D \frac{\sin\left(k|\mathbf{r}-\mathbf{r}'|\right)}{|\mathbf{r}-\mathbf{r}'|} f^*(\mathbf{r}') d\mathbf{r}'. \end{aligned} \tag{88}$$

In particular, for a point source $f(\mathbf{r}) = \delta(\mathbf{r} - \mathbf{r}_0)$, we have

$$v(\mathbf{r}) = \frac{1}{2\pi i} \frac{\sin(k|\mathbf{r} - \mathbf{r}_0|)}{|\mathbf{r} - \mathbf{r}_0|}.$$

In this case, the time reversal resolution is proportional to λ. Note that (88) is independent of the domain D as long as it contains the support of f.

B. Paraxial wave

Next, we consider time reversal in a random medium. For simplicity we use the Markovian model.

Here, a source $\Psi_0(\mathbf{x})$ located at $z = L$ emits a signal with the carrier wavenumber k toward the time reversal mirror (TRM) of aperture A located at $z = 0$ through a turbulent medium. The transmitted field is captured and time reversed at the TRM and then sent back toward the source point through the same turbulent medium, [25], [26].

The time-reversed, back-propagated wave field at $z = L$ can be expressed as

$$\begin{aligned} \Psi_{\mathrm{tr}}(\mathbf{x}) &= \int G(L, \mathbf{x}, \mathbf{x}_m) G^*(L, \mathbf{x}_s, \mathbf{x}_m) \Psi_0^*(\mathbf{x}_s) \mathbb{I}_A(\mathbf{x}_m) d\mathbf{x}_m d\mathbf{x}_s \\ &= \int e^{i\mathbf{p}\cdot(\mathbf{x}-\mathbf{x}_s)/\gamma} W(L, \frac{\mathbf{x}+\mathbf{x}_s}{2}, \mathbf{p}) \Psi_0^*(\mathbf{x}_s) d\mathbf{p} d\mathbf{x}_s \end{aligned} \tag{89}$$

where $\mathbb{I}_A$ is the indicator function of the TRM, G the propagator of the Schrödinger equation and W the mixed-state Wigner distribution function

$$\begin{aligned} W(z, \mathbf{x}, \mathbf{p}) &= \int W(z, \mathbf{x}, \mathbf{p}; \mathbf{x}_m) \mathbb{I}_A(\mathbf{x}_m) d\mathbf{x}_m \\ W(z, \mathbf{x}, \mathbf{p}; \mathbf{x}_m) &= \frac{1}{(2\pi)^2} \int e^{-i\mathbf{p}\cdot\mathbf{y}} G(z, \mathbf{x} + \gamma\mathbf{y}/2, \mathbf{x}_m) G^*(z, \mathbf{x} - \gamma\mathbf{y}/2, \mathbf{x}_m) d\mathbf{y} \end{aligned}$$

which is the convex combination of the pure-state Wigner distributions $W(\cdot; \mathbf{x}_m)$. Here we have used the fact that time reversing of the signal is equivalent to the phase conjugating of its spatial component.

Let us consider a point source located at $(z, 0)$ by substituting the Dirac-delta function $\delta(\mathbf{x})$ for Ψ_0 in (89) and calculate $\mathbb{E}\Psi_{\mathrm{tr}}$ with the Green function (45). We then obtain the point-spread function for the time reversed, refocused wave field written as $\mathcal{P}_{tr}(\mathbf{x}) = \mathcal{P}_0(\mathbf{x}) T_{tr}(\mathbf{x})$ with

$$\begin{aligned} \mathcal{P}_0(\mathbf{x}) &\equiv \left(\frac{1}{z\gamma}\right)^2 \exp\left[i\frac{|\mathbf{x}|^2}{2\gamma z}\right] \hat{\mathbb{I}}_A\left(\frac{\mathbf{x}}{\gamma z}\right) \\ T_{tr}(\mathbf{x}) &\equiv \exp\left[-\frac{z}{\gamma^2}\int_0^1 D_*(-s\mathbf{x}) ds\right]. \end{aligned} \tag{90}$$

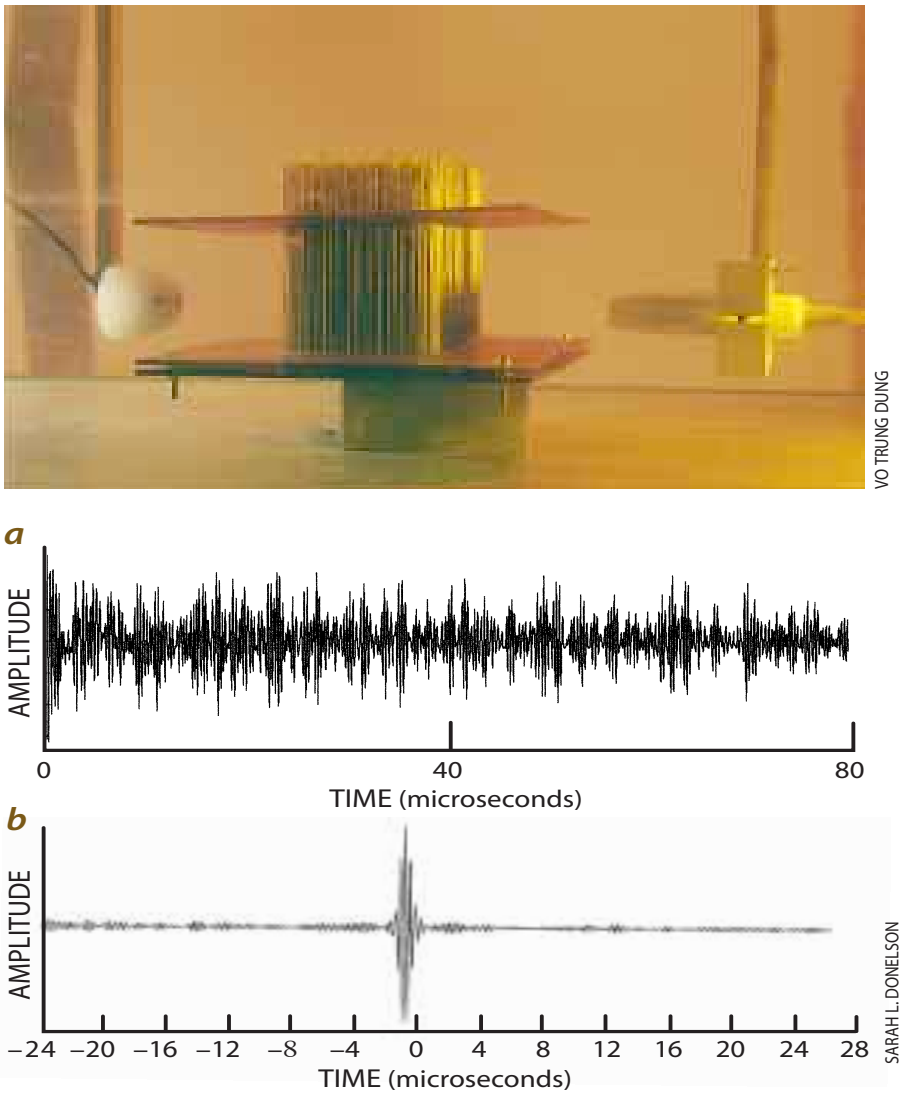

FIG. 17: Acoustic chaotic pinball occurs when an underwater ultrasonic pulse emitted by the transducer (at left in photograph) ricochets among 2,000 randomly placed steel rods before reaching the 96-element time-reversing mirror at right. Each element of the array receives a chaotic-seeming sound signal (a portion of one is shown in the middle plot) lasting much longer than the original one-microsecond pulse. When the mirror plays back the chaotic signals, reversed and in synchrony, they ricochet back through the maze of rods and combine to re-create a well-defined pulse, shown in the bottom plot, at the transducer (adapted from [28]).

In the absence of random inhomogeneity the function $T_{\rm tr}$ is unity and the resolution scale ρ_0 is determined solely by $\mathcal{P}_0$:

$$\rho_0 \sim 2\pi \frac{\gamma z}{A}. \tag{91}$$

In view of definition of γ this is evidently the classical Rayleigh resolution formula. Note that we have used the dimensionless variables.

C. Anomalous focal spot

We shall see here that a turbulent medium such as the turbulent atmosphere can significantly reduce the focal spot size below the Rayleigh limit.

To this end we assume the inertial range asymptotic:

$$D_*(r) \approx C_*^2 r^{2H_*}, \quad \ell_0 \ll r \ll L_0 = 1\,, \tag{92}$$

where the effective Hölder exponent H_* is given by

$$H_* = \begin{cases} H + 1/2 & \text{for } H \in (0, 1/2) \\ 1 & \text{for } H \in (1/2, 1) \end{cases} \tag{93}$$

and the structure parameter C_* is proportional to $\sigma_H^{1/2}$. Outside of the inertial range we have instead $D_*(r) \sim r^2, r \ll \ell_0$ and $D_*(r) \to D_*(\infty)$ for $r \to \infty$ where $D_*(\infty) > 0$ is a finite constant. As in (35) we have chosen the correlation length L_0 as the reference length L_x.

First we consider the situation where there may be an inertial range behavior. This requires from (90) that

$$\gamma^{-2} D_*(\infty) \gg 1. \tag{94}$$

In the presence of random inhomogeneities the retrofocal spot size is determined by $\mathcal{P}_0$ or $T_{\rm tr}$ depending on which has a smaller support. For the power-law spectrum we have the inertial range asymptotic

$$T_{\rm tr}(\mathbf{x}) \;\sim\; \exp\left[-C_*^2 \gamma^{-2} z |\mathbf{x}|^{2H_*} (4H_* + 2)^{-1}\right] \tag{95}$$

for $\ell_0 \ll |\mathbf{x}| \ll 1$. We define the turbulence-induced time-reversal resolution as

$$\rho_{\rm tr} = \sqrt{\int |\mathbf{x}|^2 T_{\rm tr}^2(\mathbf{x}) d\mathbf{x} \Big/ \int T_{\rm tr}^2(\mathbf{x}) d\mathbf{x}} \tag{96}$$

which by (95) has the inertial range asymptotic

$$\rho_{\rm tr} \sim \left(\frac{\gamma\lambda}{C_* \sqrt{z}}\right)^{1/H_*}, \quad \ell_0 \ll \rho_{\rm tr} \ll 1. \tag{97}$$

The nonlinear law (97) is valid only down to the inner scale ℓ_0 below which the linear law prevails $\rho_{\rm tr} \sim \gamma\lambda z^{-1/2}$.

We see that under (94) $\rho_{\rm tr}$ is independent of the aperture, has a superlinear dependence on the wavelength in the inertial range and the resolution is further enhanced as the distance z and random inhomogeneities (C_*) increase. This effect can be explained by the notion of turbulence-induced aperture which enlarges as z and C_* increase as the TRM is now able to capture signals initially propagating in the more oblique directions.

To recover the linear law previously reported in [4], let us consider the situation where $\rho_{\rm tr} = O(\gamma)$ and take the limit of vanishing Fresnel number $\gamma \to 0$ in eq. (46) by setting $\mathbf{x} = \gamma\mathbf{y}$. Then we have

$$\lim_{\gamma\to 0} \gamma^{-2} D_*(\gamma\mathbf{y}) \ = D_0|\mathbf{y}|^2, \quad D_0 \ = \frac{1}{2}\int \Phi(0,\mathbf{q})|\mathbf{q}|^2 d\mathbf{q}.$$

The resulting mean retrofocused field $\mathbb{E}\Psi_{\rm tr}(\gamma\mathbf{y})$ is Gaussian in the offset variable $\mathbf{y}$ and the refocal spot size on the original scale is given by

$$\rho_{\rm tr} \sim \gamma\lambda(D_0 z)^{-1/2}. \tag{98}$$

Hence the linear law prevails in the sub-inertial range.

D. Duality and turbulence-induced aperture

Intuitively speaking, the turbulence-induced aperture referred to in the previous section is closely related to how a wave is spread in the course of propagation through the turbulent medium. A quantitative estimation can be given by analyzing the spread of wave energy.

To this end let us calculate the mean energy density with the Gaussian initial wave amplitude

$$\Psi(0,\mathbf{x}) = \exp\left[-|\mathbf{x}|^2/(2\alpha^2)\right]. \tag{99}$$

We obtain

$$\begin{aligned}\mathbb{E}|\Psi(z,\mathbf{x})|^2 \ = \ & \left(\frac{\alpha}{2\sqrt{\pi}}\right)^d \int \exp\left[-|\mathbf{q}|^2[\alpha^2/4 + \gamma^2 z^2/(4\alpha^2)]\right] \\ & \times \exp\left[i\mathbf{q}\cdot\mathbf{x}\right] \exp\left[-\frac{z}{\gamma^2}\int_0^1 D_*(\mathbf{q}s\gamma)ds\right] d\mathbf{q}.\end{aligned}$$

The reason we do not consider the point source right away is that for a point source $\mathbb{E}|\Psi|^2 \sim$ const. so to see the effect of the random diffraction we need to consider an extensive source.

From the above the turbulence-induced spread can be identified as convolution with the kernel which is the inverse Fourier transform $\mathcal{F}^{-1}T$ of the transfer function

$$T(\mathbf{q}) = \exp\left[-\frac{z}{\gamma^2}\int_0^1 D_*(\mathbf{q}s\gamma)ds\right].$$

In view of (90), we obtain that

$$\mathcal{F}^{-1}T(\mathbf{x}) = \frac{1}{\gamma^2 z^2}\mathcal{F}^{-1}T_{\rm tr}(\frac{\mathbf{x}}{\gamma z}). \tag{100}$$

In this case it is reasonable to define the turbulence-induced forward spread σ_* as

$$\sigma_* = \sqrt{\int |\mathbf{x}|^2 \left|\mathcal{F}^{-1}T\right|^2(\mathbf{x})d\mathbf{x} / \int \left|\mathcal{F}^{-1}T\right|^2(\mathbf{x})d\mathbf{x}}$$

which, in view of (96) and (100), then satisfies the uncertainty inequality (see also [14])

$$\sigma_*\rho_{\rm tr} \geq \gamma z. \tag{101}$$

The equality holds when $T_{\rm tr}$ is Gaussian, i.e. when $H^* = 1$ or in the sub-inertial range. This strongly suggests the definition of the turbulence-induced aperture as $A_* = 2\pi\gamma\, z/\rho_{\rm tr}$ in complete analogy to (91). And we have the inequality

$$A_* \leq 2\pi\sigma_*$$

where equality holds true for a Gaussian wave structure function.

E. Coherence length

Another physical variable that is naturally dual to the wave spread is the coherence length. The physical intuition is that the larger the spread the smaller the coherence length.

In the Markovian model with the Gaussian data (99) the coherence length has the following expression:

$$\begin{aligned} &\mathbb{E}\Psi(z,\mathbf{x}+\mathbf{y}/2)\Psi(z,\mathbf{x}-\mathbf{y}/2) \\ &= \left(\frac{\alpha}{\sqrt{2\pi}}\right)^2 \int \exp\left[-|\mathbf{q}|^2\alpha^2/4\right] \exp\left[-\frac{|\mathbf{y}-\gamma z\mathbf{q}|^2}{4\alpha^2}\right] \\ &\qquad \times \exp\left[i\mathbf{q}\cdot\mathbf{x}\right] \exp\left[-\frac{1}{\gamma^2}\int_0^z D_*(-\mathbf{y}+\gamma\mathbf{q}s)ds\right] d\mathbf{q}. \end{aligned} \tag{102}$$

In the point-source limit $\alpha \to 0$, we have

$$\begin{aligned} &\mathbb{E}\Psi(z,\mathbf{x}+\mathbf{y}/2)\Psi(z,\mathbf{x}-\mathbf{y}/2) \\ &\approx \left(\frac{\sqrt{2}\alpha^2}{\gamma z}\right)^2 \exp\left[i\frac{1}{\gamma z}\mathbf{y}\cdot\mathbf{x}\right] \exp\left[-\frac{z}{\gamma^2}\int_0^1 D_*(-\mathbf{y}s)ds\right]. \end{aligned} \tag{103}$$

In view of (103) let us define the turbulence-induced coherence length δ_* as

$$\delta_* = \sqrt{\int |\mathbf{y}|^2 T_2^2(\mathbf{y})d\mathbf{y} / \int T_2^2(\mathbf{y})d\mathbf{y}}, \quad T_2(\mathbf{y}) = \exp\left[-\frac{z}{\gamma^2}\int_0^1 D_*(-\mathbf{y}s)ds\right].$$

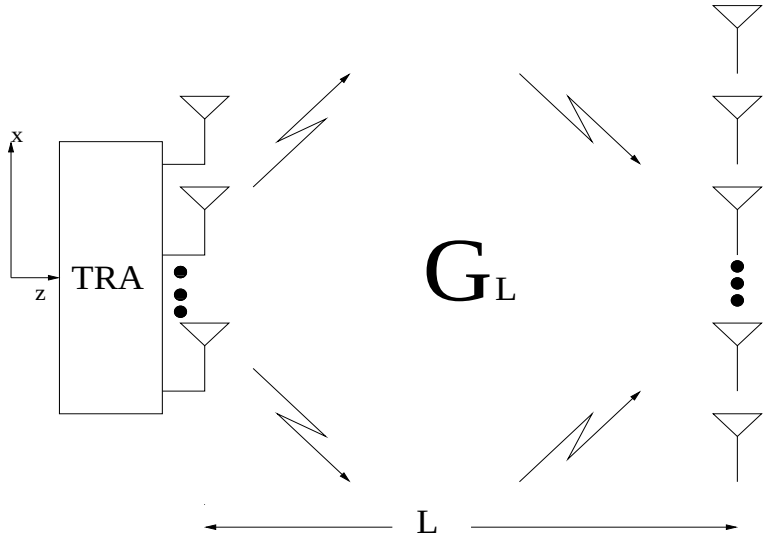

FIG. 18: MIMO Broadcast Channel

Since $T_2 = T_{\rm tr}$, δ_* is equal to the turbulence-induced time-reversal resolution $\rho_{\rm tr}$ and is related to the wave spread as

$$\sigma_* \delta_* \geq \gamma z$$

where the equality holds for a Gaussian wave structure function. Because of the identity of δ_* and $\rho_{\rm tr}$ the time reversal refocal spot size can be used to estimate the coherence length of the wave field which is more difficult to measure directly.

F. Broadband time reversal communications

Now we would like to discuss time reversal with broadband signals as a means of communication in random media. We consider the multiple-input-multiple-output (MIMO) broadcast channel described in [19], [18]. We assume that the random medium is described by the Markovian model.

Let the M receivers located at $(L, \mathbf{r}_j), j = 1, ..., M$ first send a pilot signal $\int e^{i\frac{kt}{\gamma}} g(k) dk \delta(\mathbf{r}_j - \mathbf{a}_i)$ to the N-element TRA located at $(0, \mathbf{a}_i), i = 1, ..., N$ which then use the time-reversed version of the received signals $\int e^{i\frac{kt}{\gamma}} g(k) G_L(\mathbf{r}_j, \mathbf{a}_i; k) dk$ to modulate streams of symbols and send them back to the receivers. Here G_L is the Green function of

$$i\frac{\partial \Psi_z}{\partial z} + \frac{\gamma}{2k}\Delta_{\mathbf{x}} \Psi_z + \frac{k}{\gamma}\chi_z \circ \Psi_z = 0, \quad \mathbf{x} \in \mathbb{R}^d, \tag{104}$$

and $g^2(k)$ is the power density at k. For simplicity we take $g^2(k) = \exp\left(-\frac{|k-1|^2}{2B^2\gamma^2}\right)$. As shown in [4], [10], when the TRA has an infinite time-window, the signal arriving at the receiver

plane with delay $L+t$ is given by

$$S(\mathbf{r},t) \;=\; \sum_{l=1}^{T}\sum_{i=1}^{N}\sum_{j=1}^{M} m_j(\tau_l)\int e^{-i\frac{k}{\gamma}(t-\tau_l)}g(k) \times G_L(\mathbf{r},\mathbf{a}_i;k)G_L^*(\mathbf{r}_j,\mathbf{a}_i;k)dk \tag{105}$$

where $m_j(\tau_l), l=1,...,T\leq\infty$ are a stream of T symbols intended for the j-th receiver transmitted at times $\tau_1<\tau_2<...<\tau_T$. We assume for simplicity that $|m_j(\tau_l)|=1,\ \forall j,l$.

Consider the mean $E(\mathbf{r},t)=\gamma^{-d}\int f((\mathbf{x}-\mathbf{r})/\ell_c)\mathbb{E}S(\mathbf{x},t)d\mathbf{x}$ and the variance

$$V(\mathbf{r},t)=\gamma^{-2d}\mathbb{E}\big[\int f((\mathbf{x}-\mathbf{r})/\ell_c)S(\mathbf{x},t)d\mathbf{x}\big]^2-E^2(\mathbf{r},t)$$

where the coupling with the test function f can be viewed as the averaging induced by measurement. We have made the test function f act on the scale of the coherence length ℓ_c, the smallest spatial scale of interest (the speckle size) in the present context. Different choices of scale would not affect the conclusion of our analysis.

The primary object of our analysis is

$$\rho=\frac{E^2(\mathbf{r}_j,\tau_l)}{V(\mathbf{r},t)},\quad j=1,...,M, l=1,...,T \tag{106}$$

which is the signal-to-interference ratio (SIR) if $\mathbf{r}=\mathbf{r}_j, t=\tau_l$ and the signal-to-sidelobe ratio (SSR) if $|\mathbf{r}-\mathbf{r}_j|\gg\ell_c,\forall j$ (spatial sidelobes) or $|t-\tau_l|\gg B^{-1},\forall l$ (temporal sidelobes) (as $V(\mathbf{r},\tau)\approx E^2(\mathbf{r},\tau)$ as we will see below). We shall refer to it as the signal-to-interference-or-sidelobe ratio (SISR). In the special case of $\mathbf{r}=\mathbf{r}_j$ *and* $|t-\tau_l|\gg B^{-1}$,$\forall l$, ρ^{-1} is a measure of intersymbol interference. To show stability and resolution, we shall find the precise conditions under which $\rho\to\infty$ and $\mathbb{E}S(\mathbf{r},t)$ is asymptotically $\sum_{l=1}^{T}\sum_{j=1}^{M}m_j(\tau_l)S_{jl}(\mathbf{r},t)$ where

$$S_{jl}(\mathbf{r},t)\;\approx\;\sum_{i=1}^{N}\int e^{-i\frac{k(t-\tau_l)}{\gamma}}g(k)\mathbb{E}\big[G_L(\mathbf{r},\mathbf{a}_i;k)G_L^*(\mathbf{r}_j,\mathbf{a}_i;k)\big]dk \tag{107}$$

is a sum of δ-like functions around $\mathbf{r}_j$ and $\tau_l=0,\forall l$. In other words, we employ the TRA as a multiplexer to transmit the M scrambled data-streams to the receivers and we would like to turn the medium into a demultiplexer by employing the broadband time reversal technique.

Provided that the antenna spacing is greater than the coherence length and the frequency separation is greater than the coherence bandwidth, the sufficient condition for achieving the desired goal (i.e. stability and refocusing) is the multiplexing condition

$$NB\gg MC \tag{108}$$

where C is the number of symbols per unit time in the datum streams intended for each receiver [19], [18]. The proof makes a nontrivial use of the asymptotic solution (64).

In terms of resolution, the best experimental result in this direction so far has been achieved by [42].

VII. APPLICATION: IMAGING IN RANDOM MEDIA

A. Imaging of phase objects

Consider the electron transmission microscope whose image formation is based on the interaction of electrons with the object. Two kinds of scattering are involved: elastic and inelastic scattering. The former involves no transfer of energy and give rise to high-resolution information. The latter involves transfer of energy and produces low resolution information. The electron microscopy mainly uses the former for imaging.

In most applications, the elastic scattering interaction can be described as phase shift as in (21). For weak phase object, the Born approximation $\Psi = \Psi_0(1 + i\Phi)$ is valid [32]. The Fraunhoffer diffraction can be used since the observation is always made in the far distance from the object and close to the optical axis. In that approximation the wave function in the back focal plane of the objective lens is – in the absence of aberration – the Fourier transform of u. However, the lens aberrations and the defocusing have the effect of shifting the phase of the scattered wave by an amount expressed by $2\pi\chi(\mathbf{k})$ where χ is called the wave aberration function. In a polar coordinate system $(|\mathbf{k}|, \phi)$ we have [32]

$$\chi(k, \phi) = -\frac{1}{2}\lambda\Big[\Delta z + \frac{z_0}{2}\sin(2\phi)\Big]|\mathbf{k}|^2 + \frac{1}{4}\lambda^3 C_s|\mathbf{k}|^4$$

where λ is the electron wavelength; Δz the defocus of the objective lens; z_a the focal difference due to axial astigmatism; C_s the third-order spherical aberration constant.

An ideal lens will transform an incoming plane wave into a spherical wave front converging into a single point on the back focal plane. Lens aberrations have the effect of deforming the spherical wave front. In particular, the spherical aberration term C_s acts in a way that the outer zones of the wave front are curved more than the inner zones, leading to a decreased focal length in the outer zones.

The above discussion leads to the wave function

$$\Psi_b(\mathbf{k}) = \mathfrak{F}[\Psi](\mathbf{k})e^{i2\pi\chi(\mathbf{k})}$$

in the back focal plane of the objective lens. Next, the wave function in the image plane is obtained from the wave in the back focal plane, after modification by the aperture function $A(\mathbf{k})$, through an inverse Fourier transform

$$\Psi_i(\mathbf{y}) = \mathfrak{F}^{-1}[\mathfrak{F}[\Psi](\mathbf{k})A(\mathbf{k})e^{i2\pi\chi(\mathbf{k})}]$$

where $A(\mathbf{k})$ can be taken as the indicator function of the aperture:

$$A(\mathbf{k}) = \begin{cases} 1, & \text{for} \quad |\mathbf{k}| \le \theta_1/\lambda \\ 0, & \text{else} \end{cases}$$

where θ_1 is the angle corresponding to the radius of the objective aperture. Finally, the observed intensity in the image plane is

$$I(\mathbf{y}) = |\Psi_i|^2(\mathbf{y}).$$

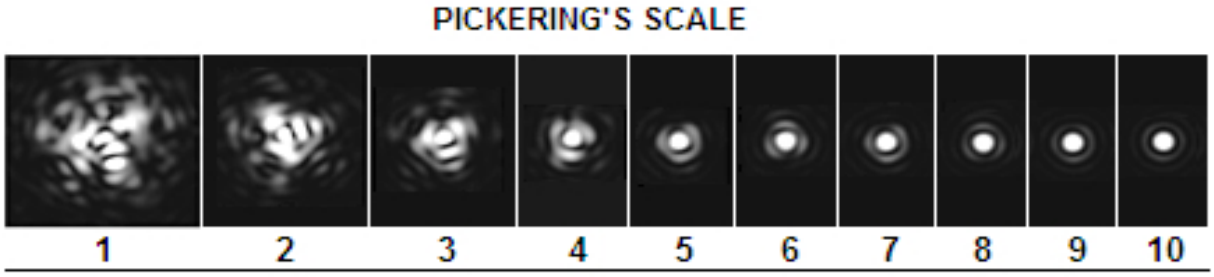

FIG. 19: Pickering's scale of rating atmospheric turbulence: the photographs show the image (intensity distribution) of a star under various atmospheric conditions.

If we apply the Born approximation, assume Φ is real-valued and subtract the constant background to consider only the contrast of the image intensity, then we obtain a linear relationship between $O(\mathbf{k}) = \mathfrak{F}[\Phi](\mathbf{k})$ and the Fourier transform of the image contrast $\mathfrak{F}[I](\mathbf{k})$:

$$\mathfrak{F}[I](\mathbf{k}) = O(\mathbf{k})A(\mathbf{k})\sin(2\pi\chi(\mathbf{k}))$$

or equivalently

$$I(\mathbf{y}) = \int \Phi(\mathbf{y}')h(\mathbf{y}-\mathbf{y}')d\mathbf{y}'$$

where $h(\mathbf{y}) = \mathfrak{F}[A(\mathbf{k})\sin(2\pi\chi)]$ is called the point-spread function of the imaging system. The function $\sin 2\pi\chi$ is known as the phase contrast transfer function and the function $A(\mathbf{k})\sin(2\pi\chi)$ is the optical transfer function.

Optical imaging systems are often built out of lens, pinholes and mirrors. For optical waves many objects can be treated as phase objects such as thin sheets or organic specimens, air flows, vortices and shock waves, strains in transparent materials, density changes in heating. The basic configuration of, for example, a microscope has 2 lenses of $4f$ geometry which is equivalent to iterated (windowed) Fourier transforms and produces an inverted image. Then the imaging quality of the system is determined by the point-spread function. The intensity of the image is the convolution of the object intensity and the point-spread function.

B. Long-exposure imaging

The refractive index fluctuation in the turbulent atmosphere restricts the angular resolution of large, ground-based telescopes to the seeing limit of 0.5 arcsec. On the other hand, the theoretical resolution of a 5m telescope is about 0.02 arcsec at wavelength 0.5μm. This is more than 20 times of reduction in resolving power.

The seeing quality can be rated by Pickering's scale which ranges from P-1(worst) to P-10 (best), Fig. 19. The Pickering scale is based on what a highly magnified star looks like when carefully focused, in a small telescope. A star at high magnification, under perfect seeing

(P-10) looks like a bull's eye. A small central disk surrounded by one or more concentric rings. At P-1, it is just an amorphous blob. The central disk is known as the Airy disk and it's size in inversely proportional to the size of the telescope objective.

Consider an object such as a faraway star or galaxy. The wave field incident on the top of the atmosphere is Ψ_0. For simplicity we consider spatially incoherent object i.e. $\langle \Psi(\mathbf{x}_1)\Psi^*(\mathbf{x}_2)\rangle = |\Psi(\mathbf{x}_1)|^2\delta(\mathbf{x}_1 - \mathbf{x}_2)$ where $\langle\cdot\rangle$ denotes the averaging w.r.t. the random phase of the object and is independent of the averaging w.r.t. the medium ensemble. In the case of a single star the wave field is nearly a plane wave. Let $G_L(\mathbf{x}, \bar{\mathbf{x}})$ be the Green function for the turbulent medium of thickness L. The wave field impinging on the lens is $\int G_L(\mathbf{x}, \bar{\mathbf{x}})\Psi_0(\bar{\mathbf{x}})d\bar{\mathbf{x}}$. The lens introduces a phase factor of the form $e^{-\frac{i}{2\gamma f}|\mathbf{x}|^2}$ and on the focal plane the wave field is given by

$$\Psi(\mathbf{x}) = e^{-\frac{i}{2\gamma f}|\mathbf{x}|^2} \int \Psi_0(\bar{\mathbf{x}})G_L(\mathbf{x}', \bar{\mathbf{x}})\mathbb{I}_A(\mathbf{x}')e^{\frac{i}{f\gamma}\mathbf{x}\cdot\mathbf{x}'}d\mathbf{x}'d\bar{\mathbf{x}} \tag{109}$$

where $\mathbb{I}_A(\mathbf{x}')$ is the indicator function of the lens. The observed intensity is then

$$I(\mathbf{x}) = \int |\Psi_0(\bar{\mathbf{x}})|^2 G_L(\mathbf{x}'_1, \bar{\mathbf{x}})G_L^*(\mathbf{x}'_2, \bar{\mathbf{x}})\mathbb{I}_A(\mathbf{x}'_1)\mathbb{I}_A(\mathbf{x}'_2)e^{\frac{i}{f\gamma}\mathbf{x}\cdot(\mathbf{x}'_1-\mathbf{x}'_2)}d\mathbf{x}'_1d\mathbf{x}'_2d\bar{\mathbf{x}} \tag{110}$$

Without the complete knowledge of G_L it is difficult to solve the basic imaging equation (110) and recover the impinging wave field Ψ_0 from the observed intensity I.

Now let us consider the long-exposure imaging equation for a spatially incoherent object. Assuming the ergodicity of the turbulent medium, after sufficiently long exposure, the intensity in the focal plane is the statistical average:

$$\mathbb{E}I(\mathbf{x}) \;=\; \int |\Psi_0(\bar{\mathbf{x}})|^2 e^{\frac{i}{f\gamma}\mathbf{x}\cdot(\mathbf{x}'_1-\mathbf{x}'_2)}\Gamma_2(L, \mathbf{x}'_1 - \mathbf{x}'_2; 0)\mathbb{I}_A(\mathbf{x}'_1)\mathbb{I}_A(\mathbf{x}'_2)d\mathbf{x}'_1d\mathbf{x}'_1d\bar{\mathbf{x}}. \tag{111}$$

Let

$$I_0(\mathbf{x}) = \frac{1}{L^2}\int e^{\frac{i}{2L\gamma}\left(\mathbf{x}_1-\mathbf{x}_2\right)\cdot\left(\mathbf{x}_1+\mathbf{x}_2-2\bar{\mathbf{x}}\right)}|\Psi_0(\bar{\mathbf{x}})|^2 e^{\frac{i}{f\gamma}\mathbf{x}\cdot(\mathbf{x}'_1-\mathbf{x}'_2)}\mathbb{I}_A(\mathbf{x}'_1)\mathbb{I}_A(\mathbf{x}'_2)d\mathbf{x}'_1d\mathbf{x}'_1d\bar{\mathbf{x}}.$$

be the intensity in the absence of the turbulent medium. Then in view of (47) we can write eq. (111) in the form

$$\mathbb{E}I(\mathbf{x}) = \int S(\mathbf{x} - \mathbf{x}')I_0(\mathbf{x}')d\mathbf{x}'$$

where

$$S(\mathbf{x}) = \int e^{-\frac{L}{\gamma^2}\int_0^1 D_*(s(\mathbf{x}'_2-\mathbf{x}'_1))ds}e^{\frac{i}{f\gamma}\mathbf{x}\cdot(\mathbf{x}'_1-\mathbf{x}'_2)}d\mathbf{x}'_1d\mathbf{x}'_2$$

represents the turbulence-induced pattern of a point source. For the purpose of imaging, the entire propagation modeling is to supply this function S.

More realistically the inversion problem should be posed with inclusion of noise:

$$\mathbb{E}I(\mathbf{x}) = \int S(\mathbf{x}-\mathbf{x}')I_0(\mathbf{x}')d\mathbf{x}' + N(\mathbf{x})$$

or in the Fourier domain

$$\mathbb{E}\hat{I}(\mathbf{k}) = \hat{S}(\mathbf{k})\hat{I}_0(\mathbf{k}) + \hat{N}(\mathbf{k}).$$

If we write the solution of the inversion problem as

$$\tilde{I}_0(\mathbf{k}) = \hat{T}(\mathbf{k})\mathbb{E}I(\mathbf{k})$$

then T can be determined from minimizing the mean-squared error

$$E = \int \mathbb{E}|\hat{I}_0(\mathbf{k}) - \tilde{I}_0(\mathbf{k})|^2 d\mathbf{k}$$

where $\langle\cdot\rangle$ stands for the average w.r.t. noise. The minimizer is called the Wiener fileter and is given by

$$\hat{T}(\mathbf{k}) = \frac{\hat{S}^*(\mathbf{k})}{|\hat{S}|^2(\mathbf{k}) + \mathrm{SSR}^{-1}}$$

where SSR stands for the signal-to-noise ratio

$$\mathrm{SSR} = \frac{|\mathbb{E}\hat{I}(\mathbf{k})|^2}{\mathbb{E}|\hat{N}(\mathbf{k})|^2}.$$

In the limit of vanishing noise, the Wiener filter reduces to the inverse filter while in the large noise limit it reduces to the matched filter. Other solutions to the inverse problem in the presence of noise can be obtained by the maximum likelihood method which seeks to maximize the likelihood function $\mathbb{P}(\mathbb{E}I\Big|\hat{I}_0)$ under the assumption of independent Poisson or Gaussian noise [1].

C. Short-exposure imaging

The limitations on long-exposure imaging with a thin lens may be quite severe. In the case of atmospheric imaging, this is mainly due to the phase distortion which causes imperfect focus. A natural approach for circumventing the problem is to use an imaging method which is insensitive to phase distortion. This is the essence of interferometric imaging techniques which in their simplest forms, produce images of the object autocorrelation function rather than the object itself. One technique is called the amplitude interferometry explainable in terms of the Michelson stellar interferometer, see Fig. 20.

A related technique is called the speckle interferometry. The general procedure is to take a long series of short exposures and find the spatial power spectrum of the image [1]. The

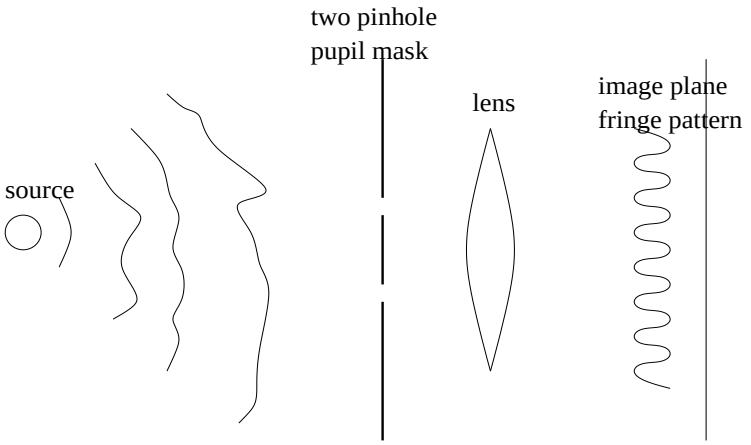

FIG. 20: Michelson interferometry

advantage of the speckle interferometry over the simple two-pinhole amplitude interferometry is that the former measures all angular frequencies simultaneously.

The assumptions are that the *phase* of the light wave from the source obeys the Gaussian statistics and the object is small enough to be contained in an atmospheric coherence area. The latter ensures the isoplanicity condition to be satisfied and implies the following simpler form than (110)

$$I(\mathbf{x}) = \int S_s(\mathbf{x} - \mathbf{x}')I_0(\mathbf{x}')d\mathbf{x}' \tag{112}$$

where S_s changes with each realization of turbulent media. After Fourier transform, we have

$$\hat{I}(\mathbf{k}) = \hat{S}_s(\mathbf{k})\hat{I}_0(\mathbf{k}).$$

Squaring modulus and averaging over a large number of short exposures we then have

$$\mathbb{E}|\hat{I}(\mathbf{k})|^2 = \mathbb{E}|\hat{S}_s(\mathbf{k})|^2|\hat{I}_0(\mathbf{k})|^2. \tag{113}$$

which can be solved by various inversion techniques once $\mathbb{E}|\hat{S}_s(\mathbf{k})|^2$ is known. In view of the discussion on the general linear inversion problem, we see that the isoplanicity assumption can be relaxed. To recover the phase of $\hat{I}_0$ we need to employ a phase retrieval technique, see [9] and [57].

The success of the method depends on the relative insensitivity of $\mathbb{E}|\hat{S}_s(\mathbf{k})|^2$ to the random phase distortion, i.e. $\mathbb{E}|\hat{S}_s(\mathbf{k})|^2$ is significantly greater than $|\mathbb{E}\hat{S}_s(\mathbf{k})|^2$. When the phase of the light wave obeys the Gaussian statistics it can be shown that $\mathbb{E}|\hat{S}_s(\mathbf{k})|^2$ is proportional to that of the homogeneous case for large value of $\mathbf{k}$. As a consequence, the speckle interferometry can yield near-diffraction-limited resolution. The effect of the large intensity fluctuations on the resolution of speckle interferometry is less clear [1].

Speckle masking is a triple correlation imaging technique which retains the phase information [57]. The quantity considered is the bispectrum

$$\mathbb{E}\hat{I}^{(3)}(\mathbf{k},\mathbf{k}') = \mathbb{E}\Big[\hat{I}(\mathbf{k})\hat{I}(\mathbf{k}')\hat{I}(-\mathbf{k}-\mathbf{k}')\Big].$$

It follows that

$$\mathbb{E}\hat{I}^{(3)}(\mathbf{k},\mathbf{k}') = \mathbb{E}\hat{S}_s^{(3)}(\mathbf{k},\mathbf{k}')\hat{I}_0^{(3)}(\mathbf{k},\mathbf{k}'). \tag{114}$$

The function $\hat{I}_0^{(3)}(\mathbf{k},\mathbf{k}')$ is the bispectrum of the object in the absence of the turbulent medium provided that we have infinite lens aperture. The function $\mathbb{E}\hat{S}_s^{(3)}(\mathbf{k},\mathbf{k}')$ is known as the speckle masking transfer function and can be derived from the speckle interferograms of a point source or it can be calculated theoretically.

By (114) the phase $\phi_0^{(3)}$ of $\hat{I}_0^{(3)}$ can be determined from $\mathbb{E}\hat{I}^{(3)}(\mathbf{k},\mathbf{k}')$ and $\mathbb{E}\hat{S}_s^{(3)}(\mathbf{k},\mathbf{k}')$. Writing

$$\hat{I}_0(\mathbf{k}) = |\hat{I}_0(\mathbf{k})|e^{i\phi_0(\mathbf{k})}$$

we obtain

$$\phi_0^{(3)}(\mathbf{k},\mathbf{k}') = \phi_0(\mathbf{k}) + \phi_0(\mathbf{k}') + \phi_0(-\mathbf{k}-\mathbf{k}') \tag{115}$$

from which a recursion relation relating ϕ_0 to $\phi^{(3)}$ can be developed. Eq. (115) is called a closure phase relation. Since the speckle masking transfer function is greater than zero up to the diffraction cutoff frequency, the diffraction-limited resolution can be achieved by the speckle masking method [57].

D. Coherent imaging of multiple point targets in Rician media

A Rician (fading) medium is a random medium whose mean or coherent component is non-vanishing and whose fluctuations obey a Gaussian distribution. Such a model is widely used in wireless literature to describe certain wireless communication channels. The Rician factor K of a Rician medium is the ratio of signal power in coherent component over the fluctuating power. Typically a Rician channel arises when there is a line-of-sight between the antennas and the targets. On the other hand, for a richly scattering environment, the coherent component is so dim that $K \approx 0$ effectively. Such a medium is called Rayleigh fading. Clearly Rayleigh media pose a greater challenge to imaging obscured targets than Rician media. In this section, we discuss the theory and practice of imaging multiple point targets in a Rician medium. For more details, the reader is referred to [27] and the references therein. We discuss briefly the case with Rayleigh media in the next section.

There are two main ingredients in this theory: the first is time reversal and averaging with the mean (coherent) Green function at various frequencies; the second is the method of differential fields. We consider two kinds of arrays: the passive array when the targets are point sources and the active array when the targets are scattering objects. The differential field method is used only in the active case.

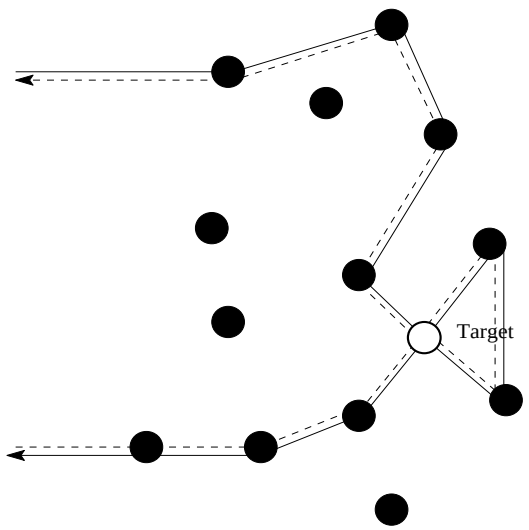

FIG. 21: Double-passage interpretation of differential field.

1. Differential scattered field in clutter

Consider the reduced wave equation with a randomly heterogeneous background

$$\Delta u_0(\mathbf{x}) + k^2 \mu_0 \varepsilon_0(\mathbf{x}) u_0 = S \tag{116}$$

where μ_0 is the magnetic permeability assumed to be unity, ε_0 the dielectric constant representing the random medium and S the source of illumination.

Suppose there is intrusion of a foreign object and as a result, the total dielectric constant $\varepsilon(\mathbf{x})$ is given by $\varepsilon_0(\mathbf{x}) + \tilde{\epsilon}(\mathbf{x})$ where $\tilde{\epsilon}(\mathbf{x})$ is a localized function representing the intrusion. Then with the same illumination the resulting electric field u satisfies

$$\Delta u(\mathbf{x}) + k^2 \big(\varepsilon_0(\mathbf{x}) + \tilde{\epsilon}(\mathbf{x})\big) u = S. \tag{117}$$

The differential (scattered) field, defined as $\tilde{u} = u - u_0$, then satisfies

$$\Delta \tilde{u}(\mathbf{x}) + k^2 \varepsilon_0(\mathbf{x}) \tilde{u} \;=\; -k^2 \tilde{\epsilon} u. \tag{118}$$

Let $\mathcal{H}_0$ and $\mathcal{H}$ be the transfer operators associated with eq. (116) and (117) respectively. Namely, $u_0 = \mathcal{H}_0 S$ and $u = \mathcal{H} S$. By (118) we can write

$$\tilde{u} = -k^2 \mathcal{H}_0 \big[\tilde{\epsilon} \mathcal{H} S\big]$$

One can visualize the multiple scattering events by noting the following perturbation expansion

$$\mathcal{H} = \Big(1 - k^2 \mathcal{H}_0 \tilde{\epsilon} + k^4 \big(\mathcal{H}_0 \tilde{\epsilon}\big)^2 - k^6 \big(\mathcal{H}_0 \tilde{\epsilon}\big)^3 + \cdots \Big) \mathcal{H}_0 \tag{119}$$

from which we obtain the expansion for the differential field

$$\tilde{u} = -k^2\mathcal{H}_0\tilde{\epsilon}\mathcal{H}_0 S + k^4\mathcal{H}_0\big(\tilde{\epsilon}\mathcal{H}_0\tilde{\epsilon}\big)\mathcal{H}_0 S - k^6\mathcal{H}_0\big(\tilde{\epsilon}\mathcal{H}_0\tilde{\epsilon}\mathcal{H}_0\tilde{\epsilon}\big)\mathcal{H}_0 S + \cdots \tag{120}$$

The terms in parentheses of (120) correspond the multiple scattering events between the target and the clutter.

For the simplicity we assume a weakly scattering target such that the multiple scattering between the target and the medium is negligible. This leads to the following simplification for the differential field

$$\tilde{u} = -k^2\mathcal{H}_0\tilde{\epsilon}\mathcal{H}_0 S. \tag{121}$$

In this setting, the imaging problem is to determine $\tilde{\epsilon}$ from the information about $\tilde{u}$ without detailed information about $\mathcal{H}_0$.

2. Imaging functions

For a passive array, the signals are sampled by the antenna array and phase conjugated. The imaging method consists of back-propagating the resulting signals in computation domain by using an imaging filter $P(\omega)$ related to the mean Green function at frequency ω. Let $\tau_i(\omega)$ be the strength of i-th point sources $i = 1, ..., M$. The resulting imaging field is

$$u(\mathbf{x}) = \sum_{l=1}^{B}\sum_{j=1}^{N}\sum_{i=1}^{M}\tau_i(\omega_l)P(\mathbf{x}, \mathbf{y}_j; \omega_l)H_{ij}(\omega_l).$$

We write $\mathbf{P}(\omega) = [P_{ij}(\omega)]$ with $P_{ij}(\omega) = P(\mathbf{x}_i, \mathbf{y}_j; \omega)$.

In the case of an active array, we apply the method of the differential (response) field. In this approach, probing signals of various frequencies are first used to survey the random media in the absence of targets. Then in the presence of targets (with unknown locations) the same set of probing signals are used again to survey the media which is assumed to be fixed. The differences between these two responses is called the differential response which is then used to image the targets.

Let $\tau_i(\omega)$ be the scattering strength (reflectivity) of the i-th target, $i = 1, ..., M$ at frequency ω and let $\mathbf{H} = [H_{ij}]$ be the transfer matrix between the point targets and the antenna array. We shall assume weakly scattering targets so that the multiple scattering between the targets and the clutter is negligible and the only multiple scattering effect is in the clutter. In this approximation, the differential responses are given by $\sum_{i=1}^{M}\tau_i(\omega_l)H_{ij}(\omega_l)H_{in}(\omega_l), j = 1, ..., N, l = 1, ..., B$ where the index $n = 1, ..., N$ indicates the array elements emitting the probing signals. The imaging field in this case is given by

$$u(\mathbf{x}) = \sum_{l=1}^{B}\sum_{i=1}^{M}\sum_{j,n=1}^{N}\tau_i(\omega_l)P(\mathbf{x}, \mathbf{y}_j; \omega_l)H_{ij}(\omega_l)H_{in}(\omega_l)P(\mathbf{y}_n, \mathbf{x}; \omega_l)$$

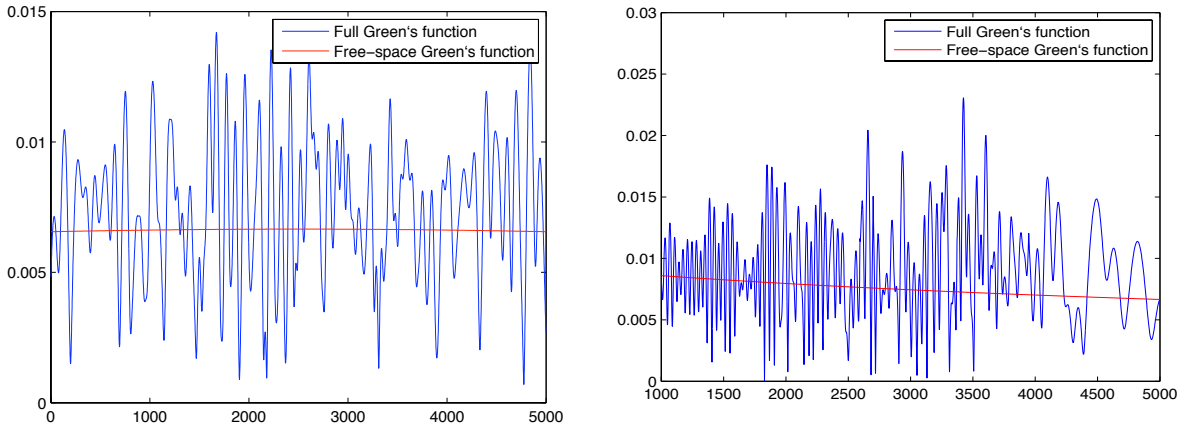

FIG. 22: Typical transverse (left) and longitudinal (right) profiles of the intensity of the Green function with 1000 randomly distributed particles corresponding to $K \sim 1$.

or more generally

$$u(\mathbf{x}) = \sum_{l=1}^{B} f(\omega_l) \sum_{i=1}^{M} \sum_{j,n=1}^{N} \tau_i(\omega_l) P(\mathbf{x}, \mathbf{y}_j; \omega_l) H_{ij}(\omega_l) H_{in}(\omega_l) P(\mathbf{y}_n, \mathbf{x}; \omega_l)$$

with a weight function f of the frequency.

One of the central questions with imaging of cluttered targets is the statistical stability. Namely, how to construct an imaging functional that is independent of a certain class of unknown, random media? For any imaging function u a useful metric of stability is the signal-to-interference ratio (SIR) of the imaging functional at the location $\mathbf{x}$ given by

$$\mathfrak{R}(\mathbf{x}) \equiv \frac{|\mathbb{E}u(\mathbf{x})|^2}{\mathbb{E}\big(|u|^2(\mathbf{x})\big) - |\mathbb{E}\big(u(\mathbf{x})\big)|^2}.$$

A statistically stable imaging function corresponds to $\mathfrak{R} \gg 1$ whenever $\mathbb{E}u(\mathbf{x}) \neq 0$ and, in particular, in the neighborhood of every target point. Under such condition, the peaks of the amplitude $|u(\mathbf{x})|$ correspond to the point targets.

Our aim is to achieve stable imaging with as little information on the full Green function as possible. A natural choice for P is the phase factor of the mean Green function of the clutter. Our main assumptions are that the antenna elements and the point targets are sufficiently separated from one another, and that the multiple frequencies used are also sufficiently separated (see [27]). Under these conditions, we show that a sufficient condition for imaging stability is $KBN \gg M$ where B is the number of frequencies, N the number of antenna elements and M the number of point targets.

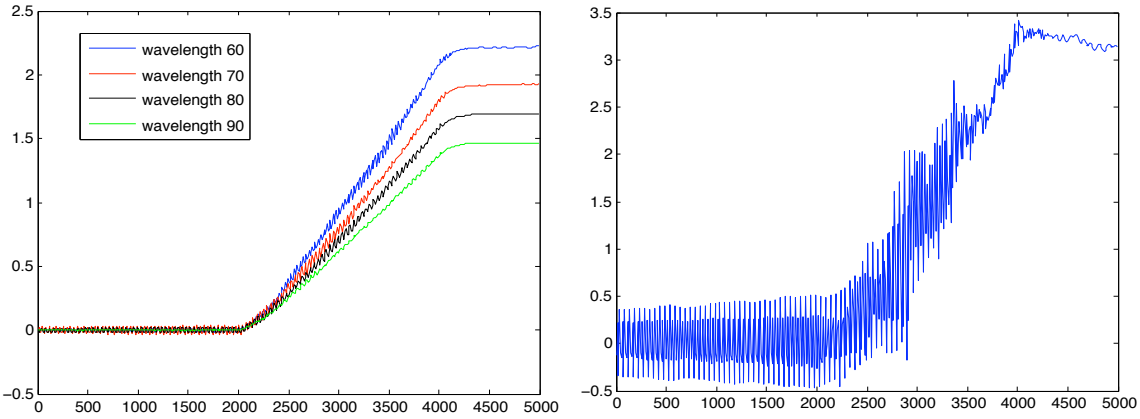

FIG. 23: The difference between the phase of the *mean* Green function, calculated with 3000 particles, and that of the free-space Green function along the longitudinal at various frequencies. The figure on the left shows linear growth of the phase difference with the propagation distance in the clutter for longer wavelengths while the figure on the right displays large fluctuations of the phase difference for wavelength 50.

3. Numerical simulation with a Rician medium

Consider a discrete medium consisting of many randomly distributed point scatterers. Multiple scattering of waves in such a medium can be conveniently simulated by using the Foldy-Lax formulation of the Lippmann-Schwinger equation [27].

In the simulations, either 1000 or 3000 point scatterers are uniformly randomly distributed in the domain $[2000, 4000] \times [0, 5000]$, while the whole computation domain is $[-5000, 5000] \times [0, 5000]$. The transverse and longitudinal profiles of the Green function are shown in Fig. 22. With 1000 particles, the K-factor in the clutter is on the order of unity.

For uniformly distributed scatterers, with a constant number density ρ, the mean Green function $\bar{H}$ in the high-frequency, forward scattering approximation satisfies the effective equation

$$\left(\nabla^2 + K_{\text{eff}}^2\right)\bar{G} = 0$$

with the effective wavenumber

$$K_{\text{eff}} = k + 2\pi f(\omega)\rho/k \tag{122}$$

where $f(\omega)$ is the forward scattering amplitude at frequency ω. By the forward scattering theorem [37], the total extinction cross section σ_t is given by

$$\sigma_t = \begin{cases} \frac{4\pi}{k}\Im[f(\omega)], & d = 3 \\ 4\Im[f(\omega)], & d = 2. \end{cases} \tag{123}$$

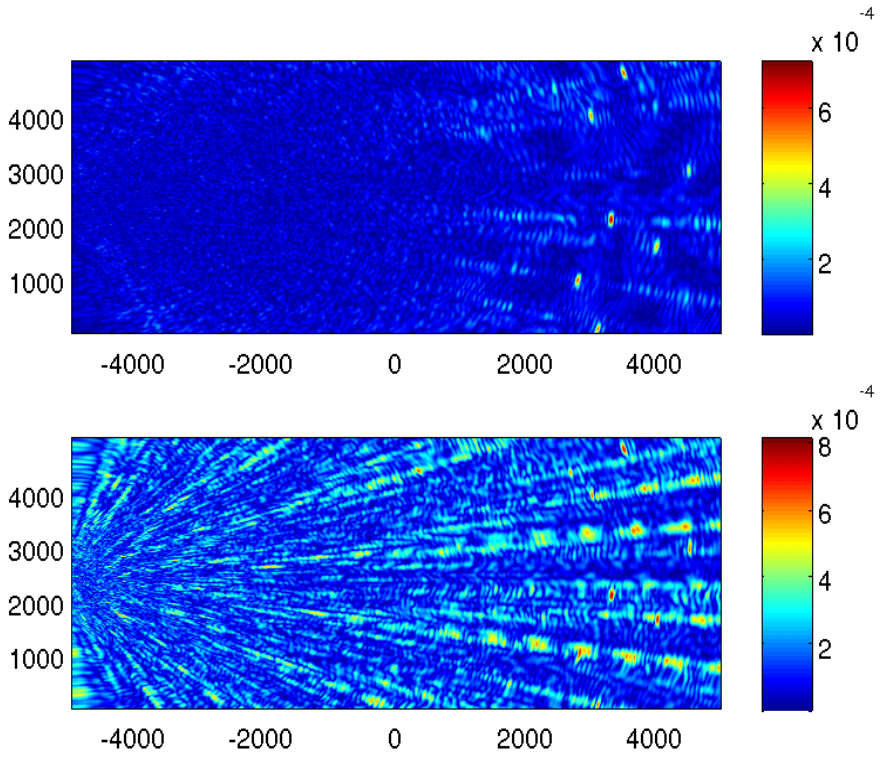

FIG. 24: Active array imaging $|u(\mathbf{x})|$ of 7 point targets located at $[3100, 100]$, $[2800, 1000]$, $[4000, 1600]$, $[3300, 2100]$, $[4500, 3000]$, $[3000, 4000]$, and $[3500, 4800]$: the top and bottom plots are simulated with 1000 and 3000 point scatterers, respectively, randomly distributed in $x \in [2000, 4000]$. The scattering strengths of an individual scatterer to a target are $70 : 1$. The 6 equally spaced antenna elements are on $y \in [1500, 3500]$, $x = -5000$. We use 20 equally spaced wavelengths from 52 to 90 and the weight function $f(\omega) = 1$.

Therefore the mean Green function in three dimensions has the form

$$\bar{G}(\mathbf{x}, \mathbf{y}; k) = -e^{-\rho\sigma_t r/2} \frac{e^{i\Re[K_{\text{eff}}]r}}{4\pi r}, \quad r = |\mathbf{x} - \mathbf{y}|. \tag{124}$$

From Fig. 23 we see that $\Re[K_{\text{eff}}]$ is linearly proportional to k with a constant only slightly larger than one.

To demonstrate the robustness of our approach, we will just use the phase factor e^{ikr} of the free-space Green function as the back-propagator P for imaging. Fig. 24 and 25 show the results with 7 obscured point targets and $f(\omega) = 1$ and $f(\omega) = \omega^{-1}$, respectively.

This simple imaging method can be easily extended to the case of extended targets. Fig. 26 shows the result with 5 line segments in both the passive and active array cases.

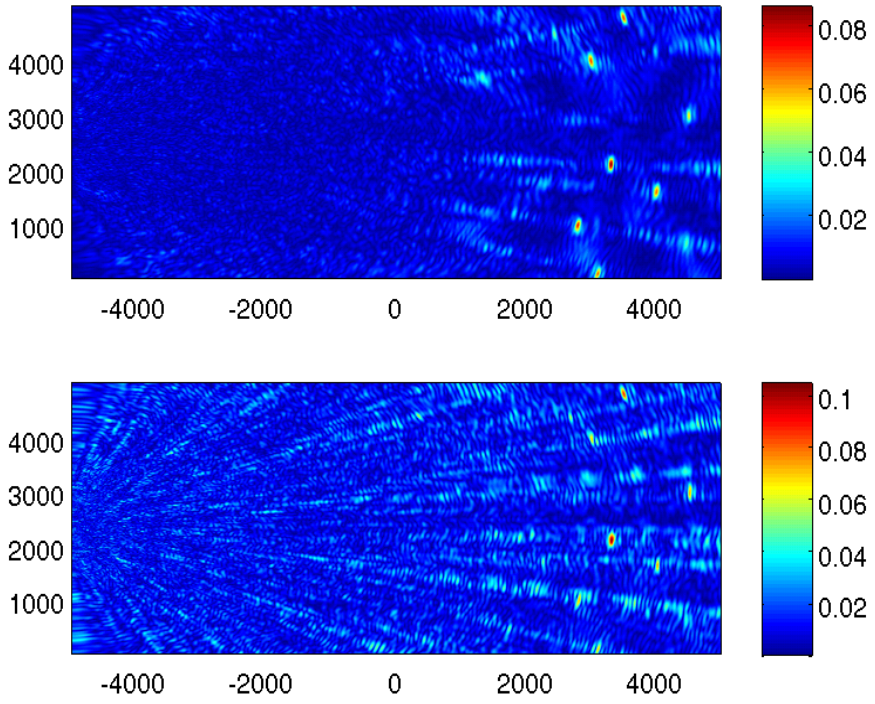

FIG. 25: The same setting as in Fig. 24 except with $f(\omega) = |\omega|^{-1}$. Compared to Fig. 24, the resolution worsens but the stability is improved.

E. Coherent imaging in a Rayleigh medium

A Rayleigh medium is characterized by a zero-mean (i.e. zero K-factor) Gaussian distributed Green function G. Physically speaking, this assumption can be expressed by $g \gg 1$, where the dimensionless conductance g is the ensemble average of the transmittance [2], [48].

When $g \gg 1$, the transfer function G possesses a dominant short-range correlation on the scale of the transport mean-free-path. If the field point separations are larger than ℓ_t we can make the approximation

$$\mathbb{E}\left[G(\mathbf{x},\mathbf{y})G^*(\mathbf{x}',\mathbf{y}')\right] \approx \mathbb{E}\left|G(\mathbf{x},\mathbf{y})\right|^2 \delta(\mathbf{x}-\mathbf{x}')\delta(\mathbf{y}-\mathbf{y}') \tag{125}$$

where $\mathbf{x}, \mathbf{x}'$ are points on the front surface X of the wall while $\mathbf{y}, \mathbf{y}'$ are points on the back surface Y.

By (125) and the rule of computing Gaussian moments we obtain the fourth-order coher-

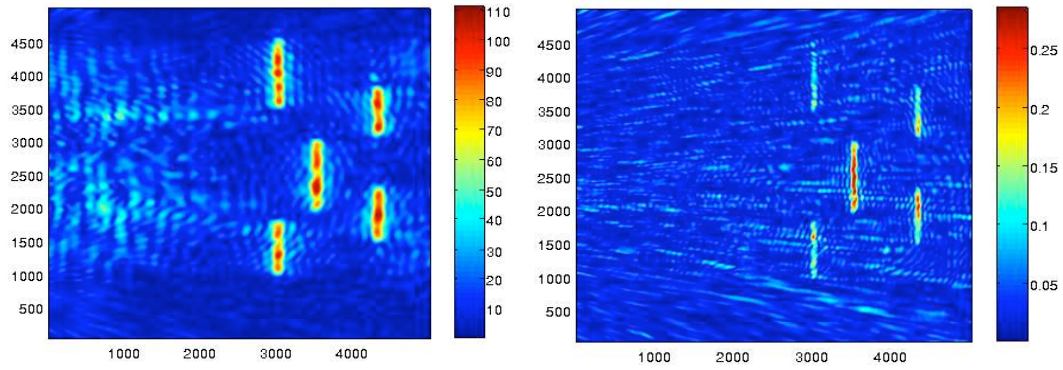

FIG. 26: Passive (left) and active (right) array imaging with 51 antennas of 5 line segments cluttered in 3000 particles. The 51 equally spaced antennas are placed on the boundary $x = -5000, y \in [0, 5000]$ (not shown). The other imaging parameters are the same as in Fig. 24.

ence function

$$\begin{aligned}
&\mathbb{E}\left[G(\mathbf{x}_1,\mathbf{y}_1)G^*(\mathbf{x}_1',\mathbf{y}_1')G(\mathbf{x}_2,\mathbf{y}_2)G^*(\mathbf{x}_2',\mathbf{y}_2')\right] \qquad (126)\\
&\approx \mathbb{E}\left[\left|G(\mathbf{x}_1,\mathbf{y}_1)\right|^2\right]\mathbb{E}\left[\left|G(\mathbf{x}_2,\mathbf{y}_2)\right|^2\right]\Big[\delta(\mathbf{x}_1-\mathbf{x}_1')\delta(\mathbf{y}_1-\mathbf{y}_1')\delta(\mathbf{x}_2-\mathbf{x}_2')\delta(\mathbf{y}_2-\mathbf{y}_2')\\
&\quad +\delta(\mathbf{x}_1-\mathbf{x}_2')\delta(\mathbf{y}_1-\mathbf{y}_2')\delta(\mathbf{x}_2-\mathbf{x}_1')\delta(\mathbf{y}_2-\mathbf{y}_1')\Big].
\end{aligned}$$

For a statistically homogeneous medium the mean angular transmission coefficient $\mathbb{E}\left|G(\mathbf{x},\mathbf{y})\right|^2$ is a function of $|\mathbf{x}-\mathbf{y}|$ and may be expressed as

$$\mathbb{E}\left|G(\mathbf{x},\mathbf{y})\right|^2 = \hat{T} f_T(|\mathbf{x}-\mathbf{y}|)$$

where the mean (total) transmission coefficient $\hat{T}$ is proportional to ℓ_t/L_c and the angular transmission density function f_G is nonnegative and normalized

$$\int f_T(r)dr = \frac{1}{2\pi}.$$

Now let us describe the imaging geometry. The array elements are assumed to have the capability of making coherent measurement as well as transmitting coherent signals. Furthermore, the array elements are assumed to be a point transmitter/receiver and separated by more than one coherence length ℓ_c of the channel, which is typically comparable to the wavelength λ, so as to form a non-redundant aperture.

The differential scattered field from the front of the target is given by

$$u(\mathbf{a};\mathbf{s}) \;=\; \int d\mathbf{x}'d\mathbf{r}d\mathbf{x}G_0(\mathbf{s},\mathbf{x})G(\mathbf{x},\mathbf{r})\tau(\mathbf{r})G(\mathbf{x}',\mathbf{r})G_0(\mathbf{a},\mathbf{x}').$$

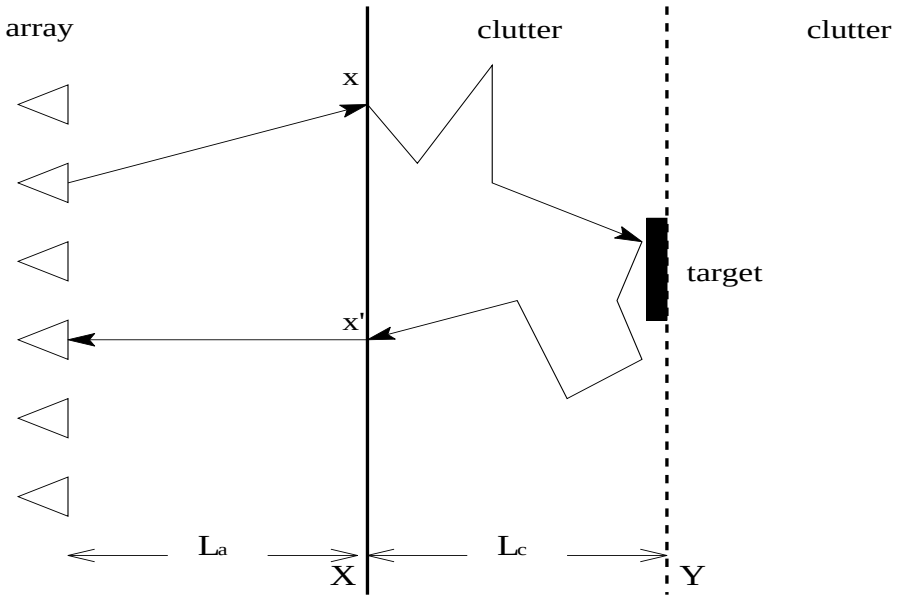

FIG. 27: Geometry for imaging the front of the cluttered target

With this we can compute the mutual coherence function of the differential scattered field

$$\begin{aligned}\mathbb{E}\left[u(\mathbf{a}_1;\mathbf{s}_1)u^*(\mathbf{a}_2;\mathbf{s}_2)\right] &= \hat{T}^2\int d\mathbf{r}\big|\tau(\mathbf{r})\big|^2\int d\mathbf{x} f_T(|\mathbf{x}-\mathbf{r}|)G_0(\mathbf{s}_1,\mathbf{x})G_0^*(\mathbf{s}_2,\mathbf{x}) \\ &\quad\times\int d\mathbf{x}' f_T(|\mathbf{x}'-\mathbf{r}|)G_0(\mathbf{a}_1,\mathbf{x}')G_0^*(\mathbf{a}_2,\mathbf{x}') \\ &+ \hat{T}^2\int d\mathbf{y}\big|\tau(\mathbf{r})\big|^2\int d\mathbf{x} G_0^*(\mathbf{a}_2,\mathbf{x})f_T(|\mathbf{x}-\mathbf{r}|)G_0(\mathbf{s}_1,\mathbf{x}) \\ &\quad\times\int d\mathbf{x}' G_0^*(\mathbf{s}_2,\mathbf{x}')f_T(|\mathbf{x}'-\mathbf{r}|)G_0(\mathbf{a}_1,\mathbf{x}').\end{aligned} \tag{127}$$

The second term in (127) represents the interference effect missing in radiative transfer theory.

We then have from (127) that

$$\begin{aligned}&[u(\mathbf{a}_1;\mathbf{s}_1)u^*(\mathbf{a}_2;\mathbf{s}_2)] \\ &= \int d\mathbf{r}\big|\tau(\mathbf{r})\big|^2\Big[F_T(\mathbf{r};\mathbf{s}_1,\mathbf{s}_2)F_T(\mathbf{r};\mathbf{a}_1,\mathbf{a}_2)+F_T(\mathbf{r};\mathbf{s}_1,\mathbf{a}_2)F_T(\mathbf{r};\mathbf{a}_1,\mathbf{s}_2)\Big]\end{aligned} \tag{128}$$

where

$$F_T(\mathbf{y};\mathbf{a},\mathbf{a}') = \int d\mathbf{x} f_T(|\mathbf{x}-\mathbf{y}|)G_0(\mathbf{a},\mathbf{x})G_0^*(\mathbf{a}',\mathbf{x}).$$

To bring (128) into more familiar form, let us assume that the clutter is in the far field such that the incident field is nearly a plane wave. Under such condition the Fraunhoffer diffraction is valid:

$$G_0(\mathbf{a},\mathbf{x}) \sim e^{-ik\mathbf{a}\cdot\mathbf{x}/L_a}$$

where L_a is the distance between the array and the wall. Unimportant constants have been ignored. Then

$$F_T(\mathbf{y};\mathbf{a},\mathbf{a}') \sim \mathfrak{F}[f_T]\big(\frac{\mathbf{a}-\mathbf{a}'}{\lambda L_a}\big)e^{-ik(\mathbf{a}-\mathbf{a}')\cdot\mathbf{y}/L_a}$$

where $\mathfrak{F}$ stands for the Fourier transform. As a consequence we obtain

$$\begin{aligned}\mathbb{E}\left[u(\mathbf{a}_1;\mathbf{s}_1)u^*(\mathbf{a}_2;\mathbf{s}_2)\right] \;\sim\; & \hat{T}^2\mathfrak{F}\big[\big|\tau\big|^2\big]\big(\frac{\mathbf{s}_1-\mathbf{s}_2+\mathbf{a}_1-\mathbf{a}_2}{\lambda L_a}\big)\Big[\mathfrak{F}[f_T]\big(\frac{\mathbf{s}_1-\mathbf{s}_2}{\lambda L_a}\big)\mathfrak{F}[f_T]\big(\frac{\mathbf{a}_1-\mathbf{a}_2}{\lambda L_a}\big)\\ & +\mathfrak{F}[f_T]\big(\frac{\mathbf{s}_1-\mathbf{a}_2}{\lambda L_a}\big)\mathfrak{F}[f_T]\big(\frac{\mathbf{a}_1-\mathbf{s}_2}{\lambda L_a}\big)\Big]. \qquad (129)\end{aligned}$$

The function $\mathfrak{F}[f_T]$ is typically exponentially decaying

$$\mathfrak{F}[f_T](\mathbf{p}) \sim \frac{L_c|\mathbf{p}|}{\sinh\big(L_c|\mathbf{p}|\big)}$$

and limits the number of accessible modes of $\mathfrak{F}[|\tau|^2]$ to up to $1/L_c$ [48]. In other words, the resolution of $\big|\tau\big|^2$ is $\sim L_c$.

---

[1] M.J. Beran and J. Oz-Vogt, *Imaging through turbulence in the atmosphere*, *Prog. Opt.* 33 (1994), 319-388.

[2] R. Berkovits and S. Feng, *Correlations in coherent multiple scattering*. *Phys. Rep.* 238 (1994), 135-172.

[3] M. Born and E. Wolf, *Principles of Optics: Electromagnetic Theory of Propagation, Interference and Diffraction of Light* (7th Edition), Cambridge University Press, 1999.

[4] P. Blomgren, G. Papanicolaou and H. Zhao, *Super-resolution in time-reversal acoustics*. *J. Acoust. Soc. Am.* 111(2002), 230.

[5] Z. Bouchal, J. Wagner and M. Chlup, *Self-reconstruction of a distorted nondiffracting beam*, *Opt. Comm.* 151 (1998) 207-211.

[6] Bruesselbach, D.C. Jones and D.A. Rockwell and R.C. Lind, *J. Opt. Soc. Am.* B 12(1995), 1434-1447.

[7] S. Chandrasekhar, *Radiative Transfer* (Dover Publications, New York, 1960).

[8] Courant and D. Hilbert, *Methods for Mathematical Physics, Vol. II.*

[9] J.C. Dainty and J.R. Fienup, *Phase retrieval and image reconstruction for astronomy*, in *Image Recovery*, ed. H. Stark, Academic Press, New York, pp, 231-275, 1987.

[10] A. Derode, E. Larose, M. Tanter, J. de Rosny, A. Tourin, M. Campillo and M. Fink, *J. Acoust. Soc. Am.*113 (2003), 2973.

[11] A. Derode, A. Tourin, J. de Rosny, M. Tanter, S. Yon, and M. Fink, *Phys. Rev. Lett.*90(2003), 014301.

[12] D. Dragoman, *The Wigner distribution function in optics and optoelectronics*, *Prog. Opt.*37(1997), 1-56.

[13] J. Durnin, *Exact solutions for nondiffracting beams. I. The scalar theory,J. Opt. Soc. Am. A* 4, 651-654 (1987).

[14] A. C. Fannjiang, *Parabolic approximation, radiative transfer and time reversal* , *J. Phys. A. Conf. Ser.* 7 (2005), 121-137.

[15] A. C. Fannjiang, *Self-averaging scaling limits for random parabolic waves. Arch. Rat. Mech. Anal.* 175:3 (2005), 343 - 387

[16] A. C. Fannjiang, *White-Noise and Geometrical Optics Limits of Wigner-Moyal Equation for Wave Beams in Turbulent Media*, *Comm. Math. Phys.* 254:2 (2005), pp. 289-322.

[17] A.C. Fannjiang, *White-Noise and Geometrical Optics Limits of Wigner-Moyal Equation for Wave Beams in Turbulent Media II. Two-Frequency Wigner Distribution Formulation*, *J. Stat. Phys.* 120 (2005), 543-586.

[18] A. Fannjiang, *Time Reversal Communication in Rayleigh Fading Broadcast Channels with Pinholes*, *Phys. Lett. A* 353/5 (2006), pp 389-397

[19] A. Fannjiang, *Information Transfer in Disordered Media by Broadband Time-Reversal: Stability, Resolution and Capacity*, *Nonlinearity* 19 (2006) 2425-2439.

[20] A.C. Fannjiang, *Space-frequency correlation of classical waves in disordered media: high-frequency and small-scale asymptotics*, *Europhys. Lett.* 80 (2007) 14005.

[21] A.C. Fannjiang, *Two-frequency radiative transfer and asymptotic solution*, *J. Opt. Soc. Am. A* 24 (2007), 2248-2256.

[22] A.C. Fannjiang, *Self-Averaging Scaling Limits of Two-Frequency Wigner Distribution for Random Paraxial Waves*, *J. Phys. A: Math. Theor.* 40 (2007) 5025-5044.

[23] A.C. Fannjiang, *Mutual Coherence of Polarized Light in Disordered Media: Two-Frequency Method Extended*, *J. Phy. A: Math. Theor.* 40 (2007) 13667-13683.

[24] A.C. Fannjiang, *Two-Frequency Radiative Transfer. II: Maxwell Equations in Random Dielectrics*, *J. Opt. Soc. Am. A* 24 (2007) 3680-3690.

[25] A.C. Fannjiang and K. Solna *Superresolution and Duality for Time-Reversal of Waves in Random Media*, *Phys. Lett. A*352:1-2 (2005), pp. 22-29.

[26] A. C. Fannjiang and K. Solna, *Propagation and Time-reversal of Wave Beams in Atmospheric Turbulence*, *SIAM Multiscale Mod. Sim.* 3:3 (2005), pp. 522-558.

[27] A.C. Fannjiang and M. Yan, *Multi-frequency imaging of multiple targets in Rician fading channels: stability and resolution*, *Inverse Problems* 23 (2007) 1801-1819.

[28] M. Fink, *Time-reversed acoustics*, *Sci. Amer.* November 1999, 91-97.

[29] M. Fink, D. Cassereau, A. Derode, C. Prada, P. Roux, M. Tanter, J.L. Thomas and F. Wu, *Rep. Progr. Phys.* 63(2000), 1933-1995.

[30] M. Fink and C. Prada, *Inverse Problems* 17 (2001), R1-R38.

[31] G.W. Forbes, V.I. Man'ko, H.M. Ozaktas, R. Simon, K.B. Wolf eds., *Wigner Distributions and Phase Space in Optics*, 2000 (feature issue, *J. Opt. Soc. Am. A* **17** No. 12).

[32] J. Frank, *Three-Dimensional Electron Microscopy of Macromolecular Assemblies*, Oxford University Press, New York, New York, 2006.

[33] A. Ghatak and K. Thyagarajan, *Graded index optical waveguide: a review. Prog. Opt.*18 (1980), 3-126.

[34] M. Gower and D. Proch, *Optical Phase Conjugation*. Springer-Verlag, Berlin, Heidelberg, 1994.

[35] F. Hlawatsch, *Time-Frequency Analysis and Synthesis of Linear Signal Spaces*, Kluwer Academic Publishers, Boston, 1998.

[36] M. Hegner, *Optics: The light fantastic*, *Nature* 419 (2002), 125-127.

[37] A. Ishimaru, *Wave Propagation and Scattering in Random Media. Vol. 1*, Academic Press, New York, 1978.

[38] A. Ishimaru, *Wave Propagation and Scattering in Random Media. Vol. 2*, Academic Press, New York, 1978.

[39] S. Jaffard, Y. Meyer and R.D. Ryan, *Wavelets – Tools for Science & Technology*, SIAM, Philadelphia, 2001.

[40] G. S. Kino, *Acoustic Waves – Devices, Imaging & Analog Signal Processing*, Prentice-Hall, Englewood Cliffs, New Jersey, 1987.

[41] W.A. Kuperman, W. Hodgkiss, H.C. Song, T. Akal, C. Ferla and D.R. Jackson, *Phase conjugation in the ocean: experimental demonstration of an acoustic time-reversal mirror. J. Acoust. Soc. Amer.* 102 (1997), 1-16.

[42] G. Lerosey, J. de Rosny, A. Tourin, M. Fink, *Focusing Beyond the Diffraction Limit with Far-Field Time Reversal, Science* 315 (2007), 1120.

[43] L. Mandel and E. Wolf, *Optical Coherence and Quantum Optics* (Cambridge University Press, 1995).

[44] C.A. McQueen, J. Arit and K. Dholakia, *An experiment to study a "nondiffracting" light beam*, *Am. J. Phys.* 67 (1999) 912-915.

[45] R. Merlin,*Radiationless Electromagnetic Interference: Evanescent-Field Lenses and Perfect Focusing Science Express*, 10.1126/science.1143884, July 12, 2007.

[46] M. Mishchenko, L. Travis, A. Lacis, *Multiple Scattering of Light by Particles: Radiative Transfer and Coherent Backscattering* (Cambridge University Press, Cambridge, 2006).

[47] F. Natterer, *The Mathematics of Computerized Tomography*, Teubner, Stuttgart, 1986.

[48] M.C.W. van Rossum and Th. M. Nieuwenhuizen, *Multiple scattering of classical waves: microscopy, mesoscopy and diffusion. Rev. Mod. Phys.* 71 (1999), 313-371.

[49] R. Sambles, *Nano-Optics: Gold loses its lustre*, *Nature* 438, 295-296 (2005)

[50] V. M. Shalaev, *Optical negative-index metamaterials Nature Photonics* 1, 41 - 48 (2007)

[51] Spohn H., *Derivation of the transport equation for electrons moving through random impurities*, *J. Stat. Phys.* 17(1977), 385-412.

[52] J.W. Strohbehn, *Laser Beam Propagation in the Atmosphere*, Springer-Verlag, Berlin, 1978.

[53] F. Tappert: *The Parabolic approximation method*, in *Wave Propagation and Underwater Acoustics*, J.B. Keller &J.S. Papadakis, eds., Lect. Notes in Phys. Vol 70, Springer-Verlag,

New York, 1977.

[54] V.I. Tatarskii, A. Ishimaru and V.U. Zavorotny, *Wave Propagation in Random Media*, SPIE, Bellingham, Washington, 1993.

[55] V.I. Tatarskii and V.U. Zavorotny, *Strong fluctuations in light propagation in a randomly inhomogeneous medium*, *Prog. Opt.*18 (1980), 205-254.

[56] A.D. Wheelon, *Electromagnetic Scintillation. Vol. II*, Cambridge University Press, Cambridge, UK, 2001.

[57] G. Weigelt, *Triple-correlation imaging in optical astronomy, Prog. Opt.* 29 (1991), 293-319.